2015

Riverine Li isotope fractionation in the Amazon River basin controlled by the weathering regimes

Mathieu Dellinger
University of Southern California

Jerome Gaillardet
Institut Universitaire de France

Julien Bouchez
Institut de Physique du Globe de Paris

Damien Calmels
Universite Paris-Sud

Pascale Louvat
Institut de Physique du Globe de Paris

See next page for additional authors

Publication Details

Dellinger, M., Gaillardet, J., Bouchez, J., Calmels, D., Louvat, P., Dosseto, A., Gorge, C., Alanoca, L. & Maurice, L. (2015). Riverine Li isotope fractionation in the Amazon River basin controlled by the weathering regimes. Geochimica et Cosmochimica Acta, 164 71-93.

Riverine Li isotope fractionation in the Amazon River basin controlled by the weathering regimes

Abstract

We report Li isotope composition (δ7Li) of river-borne dissolved and solid material in the largest River system on Earth, the Amazon River basin, to characterize Li isotope fractionation at a continental scale. The δ7Li in the dissolved load (+1.2‰ to +32‰) is fractionated toward heavy values compared to the inferred bedrock (−1‰ to 5‰) and the suspended sediments (−6.8‰ to −0.5‰) as a result of the preferential incorporation of 6Li into secondary minerals during weathering. Despite having very contrasted weathering and erosion regimes, both Andean headwaters and lowland rivers share similar ranges of dissolved δ7Li (+1.2‰ to +18‰). Correlations between dissolved δ7Li and Li/Na and Li/Mg ratios suggest that the proportion of Li incorporated in secondary minerals during weathering act as the main control on the δ7Lidiss across the entire Amazon basin. A "batch" steady-state fractionation model for Andean and lowland rivers satisfactorily reproduces these variations, with a fractionation factor between weathering products and dissolved load (αsec-disαsec-dis) of 0.983 ± 0.002. Two types of supply-limited weathering regimes can be identified for the lowlands: "clearwaters" with dominant incorporation of Li in secondary minerals, and "black waters" (e.g., Rio Negro) where dissolution of secondary minerals enhanced by organic matter produces low δ7Li. Apart from the black waters, the δ7Li of Andean and lowland rivers is negatively correlated to the denudation rates with the lowest δ7Li corresponding to the rivers having the highest denudation rates. In contrast, the main tributaries draining both the Andes and the lowlands have higher δ7Li compared to other rivers. We propose that part of the dissolved Li derived from weathering in the Andes is re-incorporated in sediments during transfer of water and sediments in floodplains and that this results in an increase of the dissolved δ7Li along the course of these rivers. Unlike other rivers, the dissolved δ7Li in the main tributaries is best described by a Rayleigh fractionation model with a fractionation factor αsec-disαsec-dis of 0.991. Altogether, the control imposed by residence time in the weathering zone and floodplain processes results in (i) a non-linear correlation between dissolved δ7Li and the weathering intensity (defined as W/D) and (ii) a positive relationship between the dissolved Li flux and the denudation rate. These results have important implications for the understanding of past ocean δ7Li and its use as a paleo weathering proxy.

Disciplines

Medicine and Health Sciences | Social and Behavioral Sciences

Publication Details

Dellinger, M., Gaillardet, J., Bouchez, J., Calmels, D., Louvat, P., Dosseto, A., Gorge, C., Alanoca, L. & Maurice, L. (2015). Riverine Li isotope fractionation in the Amazon River basin controlled by the weathering regimes. Geochimica et Cosmochimica Acta, 164 71-93.

Authors

Mathieu Dellinger, Jerome Gaillardet, Julien Bouchez, Damien Calmels, Pascale Louvat, Anthony Dosseto, Caroline Gorge, Lucia Alanoca, and Laurence Maurice

Riverine Li isotope fractionation in the Amazon River basin controlled by the weathering regimes

Mathieu Dellinger[a,b], Jerome Gaillardet[b,c], Julien Bouchez[b], Damien Calmels[d], Pascale Louvat[b], Anthony Dosseto[e], Caroline Gorge[b], Lucia Alanoca[f], Laurence Maurice[f]

[a] *Department of Earth Sciences, University of Southern California, Los Angeles, CA 90089, USA*
[b] *Institut de Physique du Globe de Paris, Sorbonne Paris Cité, Univ Paris Diderot, CNRS, F-75005 Paris, France*
[c] *Institut Universitaire de France, Paris, France*
[d] *Université Paris-Sud, Laboratoire GEOPS, UMR 8148 - CNRS, Orsay, F-91405, France*
[e] *School of Earth and Environmental Sciences, University of Wollongong, Wollongong NSW 2522, Australia*
[f] *Géosciences Environnement Toulouse, Universite Paul Sabatier, Toulouse, 31400, France*

Abstract

We report Li isotope composition (δ^7Li) of river-borne dissolved and solid material in the largest River system on Earth, the Amazon River basin, to characterize Li isotope fractionation at a continental scale. The δ^7Li in the dissolved load (+1.2‰ to +32‰) is fractionated toward heavy values compared to the inferred bedrock (-1‰ to 5‰) and the suspended sediments (-6.8 to -0.5‰) as a result of the preferential incorporation of ^{6}Li into secondary minerals during weathering. Despite having very contrasted weathering and erosion regimes, both Andean headwaters and lowland rivers share similar ranges of dissolved δ^7Li (+1.2‰ to +18‰). Correlations between dissolved δ^7Li and Li/Na and Li/Mg ratios suggest that the proportion of Li incorporated in secondary minerals during weathering act as the main control on the $\delta^7\text{Li}_{\text{diss}}$ across the entire Amazon basin. A "batch" steady-state fractionation model for Andean and lowland rivers satisfactorily reproduces these variations, with a fractionation factor between weathering products and dissolved load ($\alpha_{\text{sec}-\text{dis}}$) of 0.983. Two types of supply-limited weathering regimes can be identified for the lowlands : "clearwaters" with dominant incorporation of Li in secondary minerals, and "black waters" (e.g. Rio Negro) where dissolution of secondary minerals enhanced by organic matter produces low δ^7Li. Apart from the black waters, the δ^7Li of Andean and lowland rivers is negatively correlated to the denudation rates with the lowest δ^7Li corresponding to the rivers having the highest denudation rates. In contrast, the main tributaries draining both the Andes and the lowlands have higher δ^7Li compared to other rivers. We propose that part of the dissolved Li derived from weathering in the Andes is re-incorporated in sediments during transfer of water and sediments in floodplains and that this results in an increase of the dissolved δ^7Li along the course of these rivers. Unlike other rivers, the dissolved δ^7Li in the main tributaries is best described by a Rayleigh fractionation model with a fractionation factor $\alpha_{\text{sec}-\text{dis}}$ of 0.991. Altogether, the control imposed by residence time in the weathering zone and floodplain processes results in (i) a non-linear correlation between dissolved δ^7Li and the weathering intensity (defined as W/D) and (ii) a positive relationship between the dissolved Li flux and the denudation rate. These results have important implications for the understanding of past ocean δ^7Li and its use as a paleo weathering proxy.

Keywords: Lithium isotopes, Amazon River, Weathering, Floodplains, Denudation

1. Introduction

Silicate weathering is one of the key geological processes influencing the long-term evolution of climate through the consumption of atmospheric CO_2 (Walker et al., 1981; Berner et al., 1983). Identifying how

∗. Corresponding author
URL: mdelling@usc.edu (Mathieu Dellinger)

silicate weathering fluxes relate to potential controlling parameters is thus critical to unravel past climatic variations (Berner, 1990; Dupré et al., 2003; West et al., 2005). Conflicting results about the respective roles of climatic, tectonic and lithological parameters in setting chemical weathering fluxes have been reported (Walker et al., 1981; Raymo and Ruddiman, 1992; Gaillardet et al., 1999; West et al., 2005; Dixon and von Blanckenburg, 2012; West, 2012; Maher and Chamberlain, 2014). In order to gain insight into the respective role of these parameters, the direct quantification of paleo-weathering rates and intensities can be achieved using records of geochemical proxies for chemical weathering (e.g. Sr, Nd, Os, Be isotopes) (Raymo and Ruddiman, 1992; Willenbring and Von Blanckenburg, 2010; Li and Elderfield, 2013; Torres et al., 2014; Cogez et al., 2015). However, most of those proxies do not necessarily trace specifically past silicate weathering fluxes or intensity and a reliable geochemical weathering proxy is still lacking (Raymo and Ruddiman, 1992; Willenbring and Von Blanckenburg, 2010).

Over the last 15 years, numerous studies on soil and river water have shown that Li isotopes is a promising proxy for silicate weathering reactions (for a recent review see Burton and Vigier (2011)). This is because Li is mainly hosted in silicate minerals (Kisakurek et al., 2005; Millot et al., 2010c), while not involved in the biological turnover (Lemarchand et al., 2010) and its isotopes (^{6}Li and ^{7}Li) are fractionated by chemical weathering (Huh et al., 1998; Pistiner and Henderson, 2003). Laboratory experiments have shown that mineral dissolution produces no Li isotope fractionation (Pistiner and Henderson, 2003; Wimpenny et al., 2010a) unlike the precipitation of secondary weathering products (Vigier et al., 2008; Millot et al., 2010b) and adsorption of Li onto mineral surface phases (Zhang et al., 1998; Pistiner and Henderson, 2003; Millot and Girard, 2007). In river basins, the lithium isotope composition (δ^7Li) of the dissolved load is generally higher (by +6 to +42‰) than corresponding δ^7Li values of bedrock and suspended sediments (Kisakurek et al., 2005; Pogge von Strandmann et al., 2006, 2008; Vigier et al., 2009; Lemarchand et al., 2010; Pogge von Strandmann et al., 2010; Millot et al., 2010c; Henchiri et al., 2014). It has been suggested that the fractionation of Li isotopes in the dissolved load traces either silicate weathering intensity (Huh et al., 1998, 2001; Kisakurek et al., 2005; Pogge von Strandmann et al., 2006, 2008, 2010; Millot et al., 2010c), silicate weathering fluxes (Vigier et al., 2009), fluid residence time (Wanner et al., 2014) or exchange processes between water and sediments (Wimpenny et al., 2010b; Tipper et al., 2012; Pogge von Strandmann et al., 2012).

The recently published Li isotope seawater record over the Cenozoic by Misra and Froelich (2012) reveals a 9‰ increase of the ocean δ^7Li over the last 60 Myr. This has been interpreted as reflecting an increase of the δ^7Li of continental riverine input implying a large shift of the continental weathering regime (from "supply-limited" to "weathering-limited") as a result of increased uplift and denudation rates from early Cenozoic up to now (Misra and Froelich, 2012; Li and West, 2014; Froelich and Misra, 2014; Wanner et al., 2014). However, the parameters controlling Li isotope fractionation during chemical weathering and the link between Li isotope composition in river water and weathering regime are still poorly understood, especially at the continental scale.

Herein, we investigate the Li isotope composition of the riverine products (water and sediments) transported by the largest river system on Earth, the Amazon River. This allows us to study Li isotope fractionation by chemical weathering at a continental scale, in a relatively unpolluted area with various climatic regimes ranging from wet tropical to cold conditions, and spanning a very large range of runoffs, altitudes, bedrock types and denudation regimes. We show in particular how the weathering regime (supply vs. kinetic limitation) and the geomorphic setting (hillslopes vs. floodplains) influence the Li mass balance and therefore Li isotope fractionation. Based on these findings, we provide clues on how to interpret the Li isotope sedi-

mentary record archived in carbonates and terrigenous sediments in terms of past variations in continental weathering intensity and style.

2. Settings

The Amazon River basin is the largest river basin on Earth in terms of discharge, basin area, and one of the largest in terms of total denudation (Meade et al., 1979; Gaillardet et al., 1999). We define 4 main geomorphic areas in the Amazon Basin :

1. The Andes correspond to the Andean Cordillera where the relief ranges from about 6700 m to 500 m with steep slopes and high erosion rates. The northern part of the Andes (Peru and Ecuador) is drained by the tributaries of the Solimões River (Napo, Tigre, Morona, Pastaza, Maranon, Huallaga and Ucayali rivers) while the main tributaries of the Madeira River (Madre de Dios, Beni and Mamore rivers) drain the southern part of the Andes (Bolivia). In the Madeira basin, the lithology is relatively uniform and corresponds almost exclusively to low-grade uplifted Paleozoic silicate sedimentary rocks with a few Tertiary and Quaternary sedimentary deposits (e.g. in the Alto Beni river basin) (Stallard and Edmond, 1983; Dosseto et al., 2006b; Moquet et al., 2011). In the Solimões basin, the lithology comprises both sedimentary and igneous rocks of intermediate composition, essentially andesites in the active volcanic belt in Ecuador (Stallard and Edmond, 1983). The runoff increases from 150 mm/yr in the south (Mamore River basin) to 3400 mm/yr in the north (Moquet et al., 2011). Rivers draining the Andes are typically called the "white waters" (Gibbs, 1967) with high suspended sediment concentrations ([SPM]) from 500 to 5000 mg/L (Guyot et al., 1996; Aalto et al., 2006; Wittmann et al., 2011). The silicate weathering rates (referred here as "W") in these river basins range from 7 to 75 $t.km^{-2}.y^{-1}$ with a mean value at 22 $t.km^{-2}.y^{-1}$ for the Andean area (Moquet et al., 2011). In the Andes, the weathering regime is said to be "weathering-limited" or almost equivalently "kinetically-limited" (Stallard and Edmond, 1983), meaning that the primary minerals are not completely weathered before being eroded away (West et al., 2005).

2. The lowlands and forelands, with a relief below 500 m, have lower slopes than the Andean part and are formed by Tertiary and Quaternary sediments eroded from the Andes. Those sediments have typical PAAS-like ("Post Archean Australian Shales") composition except for some formations in the Solimões basin which have andesitic provenance signature (Roddaz et al., 2005). Rivers draining exclusively the lowlands are more diluted and have lower suspended sediment content than Andean rivers (< 100 mg/L). The silicate weathering rates of lowland rivers are generally lower than 12 $t.km^{-2}.y^{-1}$ (Moquet et al., 2011).

3. The Guyana and Brazilian shields (500-3000 m altitude) lithology corresponds essentially to the Precambrian basement formed by intermediate to acid igneous and metamorphic rocks and a few sedimentary rock outcrops. Those areas are covered by very thick soils and have very low denudation rates (Stallard and Edmond, 1983; Gaillardet et al., 1997). The [SPM] is generally no greater than 20-30 mg/L (Gaillardet et al., 1997; Moreira-Turcq et al., 2003; Wittmann et al., 2011). Two types of river water draining the shield terrains have been described by Stallard and Edmond (1983) : "clear waters" that drain lateritic (kaolinite-rich) soils and have low dissolved organic carbon content (DOC) and "black waters" draining forest areas with podzolic soils composed almost exclusively of quartz and having very high DOC content. Silicate weathering rates are very low ranging from 1 to 10 $t.km^{-1}.y^{-1}$ (Gaillardet et al., 1997; Bouchez et al., 2014).

4. Floodplains correspond to low relief environments adjacent to a stream where sediments and water deriving from the high elevation Andes are continuously deposited and exchanged with the main channel (Dunne et al., 1998; Bourgoin et al., 2007; Bouchez et al., 2012). As a result, river sediments can have a

residence time in the basin much longer than their residence time in soils (Dosseto et al., 2006a,b) and therefore be the locus of significant weathering reactions (West et al., 2002; Lupker et al., 2012; Bouchez et al., 2012; Frings et al., 2014).

River discharge and sediment fluxes of Amazon rivers are monitored by the HyBAm (Hydrology of the Amazon Basin, http ://www.ore-hybam.org) international program since more than two decade. In addition, mid-term and long-term sediment fluxes have been determined using cosmogenic radionuclides (10^3 year time scale) and fission track analyses (10^6 year time scale) (Safran et al., 2005; Wittmann et al., 2011).

3. Sampling and analytical methods

3.1. Sampling and major, trace elements concentration measurements

Water, suspended sediments and river bed sand samples were collected during several sampling cruises between 1989 and 2008. This sample set includes rivers sampled during both low and high water stages. These samples have been already characterized for major, trace element and isotope composition (Sr, Nd, U) and detailed information about analytical methods are available elsewhere (Gaillardet et al., 1997; Dosseto et al., 2006a,b; Bouchez et al., 2011, 2012). Briefly, river water samples were collected in acid-washed polypropylene containers and then filtered on site using Teflon filtration units (0.2 μm porosity). Before the analysis, the aliquots for cations, trace elements and isotope analyses were acidified with ultrapure HNO_3 to pH 2. Major anions, cations, silica and Li concentrations were measured by ion chromatography, and trace element concentrations by quadrupole ICP-MS. All samples were stored in a cold room at 4°C.

3.2. Li isotope measurements

For the dissolved load, a sample volume of 5 to 100 mL was evaporated in Teflon beakers at a temperature of about 90°C. The residue was then dissolved in 16 N distilled HNO_3 and heated at 100°C during at least 24 h to oxidise organic matter, and dried down again at 90°C. For the sediments, the acid digestion method used is described in Dellinger et al. (2014) and Li was then separated from the matrix by ion-exchange chromatography using a method modified from James and Palmer (2000) and described in Dellinger et al. (2014). Purified samples were kept until measurement as solid salts in Teflon beakers in order to avoid "ageing" of the solutions through Li adsorption or leaching of organic matter from container walls. Li isotope composition was measured using a MC-ICP-MS Neptune (Thermo Scientific, Bremen) at the laboratory of Geochemistry and Cosmochemistry at IPG Paris. Details on the analytical procedure are available in Dellinger et al. (2014). Accuracy and reproducibility of the isotopic measurements were checked through reported analyses of the IRMM-016 international standard solution, SRM rock standards, and seawater. Repeated measurements of the basalt reference materials JB-2 yielded δ^7Li = +4.47 ± 0.53‰ (±2σ, n = 30 separations and 15 digestions) and for BHVO-2, δ^7Li = +4.34 ± 0.41‰ (±2σ, n = 6 digestions). Repeated measurements of the seawater NASS-5 reference material yielded δ^7Li = +30.91 ± 0.26‰ (±2σ, n = 7 separations). Seven samples were duplicated and these duplicates agree within less than 0.60‰.

The Li concentration and isotope composition of Amazon river sediment depth-profiles have been published and discussed elsewhere (Dellinger et al., 2014). In the present study, the existing dataset has been extended to include Li concentration and isotope composition of surface SPM samples from small Beni river tributaries and shield/lowland rivers. It should be mentioned that for a few rivers, the SPM and waters analysed here have not been collected at the same time. When it is the case, it is notified in the main text or in the figures.

4. Results

4.1. Major elements in the dissolved load

Major and trace elements data are given in table (1) and agree (within 30%) with monthly time-series reported by Moquet et al. (2011). Major and trace element variability in the Amazon River has been extensively discussed elsewhere (Stallard and Edmond, 1981, 1983, 1987; Gaillardet et al., 1997; Elbaz-Poulichet et al., 1999; Mortatti and Probst, 2003; Moquet et al., 2011). Briefly, river TDS (Total Dissolved Solid) range from 2 to 200 mg/L with the lowest values for the shield rivers and some Andean catchments. Solimões tributaries draining outcrops of halite and evaporites have the highest TDS values (Stallard and Edmond, 1983; Moquet et al., 2011). Calcium (Ca) and magnesium (Mg) are always the dominant cations compared to sodium (Na) and potassium (K) except in some sodium-rich tributaries of the Solimões draining saline formations. Magnesium concentration is generally higher in the Madeira River basin (up to 350 μmol/L) compared to the Solimões River basin (maximum 100 μmol/L). Shield rivers (black and clear waters) have very low cation concentration (except for K) compared to other rivers.

4.2. Lithium concentration and isotope ratios

Dissolved lithium concentrations ($[Li]_{diss}$) in the Amazon River basin span two orders of magnitude ranging from 0.03 to 1.7 μmol/L, with a mean concentration of 0.32 μmol/L (SD=0.37, n=54) close to the worldwide riverine average of 0.27 μmol/L (Gaillardet et al., 2014; Misra and Froelich, 2012) and the original estimate of Huh et al. (1998). Our values are in good agreement with data on some Amazon tributaries published by Huh et al. (1998). The rivers draining the Amazonian shield and the Lowlands have the lowest $[Li]_{diss}$, between 0.03 and 0.12 μmol/L (Fig. 3). The major tributaries of Solimões and Madeira rivers have intermediate Li content between 0.06 and 0.60 μmol/L while the Andean rivers from the Beni River basin have the highest Li concentration (0.5 to 1.7 μmol/L).

The dissolved Li isotope composition (δ^7Li_{diss}) displays a large range of variation from +1.2 to +32.9‰ and is fractionated toward high values compared to source rocks (Fig. 2). The suspended sediments have more homogeneous δ^7Li values and are slightly enriched in ^{6}Li compared to source rocks (Fig. 2). The range of dissolved δ^7Li values is comparable to the range defined by other rivers (Li and West, 2014). The δ^7Li of the Amazon River mainstream at Óbidos ranges between +16.2 and +19.3‰ depending on the hydrological conditions. The maximum difference in δ^7Li between two samples of the same river at different times is 9.2‰ for the Negro River and 6.5‰ for the Madeira River (if we include samples from the study of Huh et al. (1998) for both rivers), 4.6‰ for the Beni River at Rurrenabaque, 3.2‰ for the Amazon River and less than 2‰ for other rivers (Tapajós, Trombetas, Madre de Dios, Mamore and Beni at Riberalta). Therefore, only the Negro and Madeira rivers show some seasonality, most likely relating to relative contributions of their tributaries. The homogeneity of the dissolved δ^7Li in the water column has been checked by measuring 3 samples collected at different depths at Óbidos, which yields similar results within analytical uncertainty (± 0.5 to 1‰). Andean rivers have lower δ^7Li_{diss} (+3.8 to +16‰) than other mountainous river (Kisakurek et al., 2005; Millot et al., 2010c). The δ^7Li of the Negro River are the lowest ever measured in running surface waters (Li and West, 2014; Wanner et al., 2014). The Mamore River has the highest δ^7Li_{diss} value of the sample set measured here (around 31‰).

A bell-shaped relationship is observed between δ^7Li_{diss} and Li concentration (Fig. 3). For rivers having $[Li]_{diss}$ lower than 0.20 μmol.L^{-1}, Li concentration is positively correlated with δ^7Li_{diss} values, while for rivers having $[Li]_{diss}$ higher than 0.20 μmol.L^{-1}, Li concentration is negatively correlated with δ^7Li_{diss}. A

clear regional distribution can be observed with rivers having common geomorphological features also sharing similar Li concentration and isotope composition. Rivers having $[Li]_{diss}$ higher than 0.4 μmol.L^{-1} correspond to the Beni River and its tributaries with δ^7Li_{diss} values systematically lower than 16‰. Shield and lowland rivers have the lowest Li concentration and display δ^7Li values from +2 to +16‰. Therefore, Andean and shield rivers, which are characterized by drastically distinct erosion and weathering conditions, display similar ranges of Li isotope composition. Finally, rivers having intermediate $[Li]_{diss}$ (0.06-0.60 μmol.L^{-1}) correspond to major tributaries of Solimões and Madeira rivers, which drain both the Andes and the lowland areas (Madre de dios, Mamore and Madeira rivers) and to the Amazon River at Óbidos. Compared to rivers draining only the Andes or the Amazonian plain, they have a much higher δ^7Li_{diss}, generally higher than 16‰.

5. Sources and isotope fractionation of Li in the Amazon River and tributaries

5.1. Partitioning of Li between dissolved and suspended loads

Following Gaillardet et al. (2014) and Bouchez et al. (2013), the proportion of lithium transported in the suspended load (e^{Li} in %) can be calculated by the Eq. (1) :

$$e^{Li} = \frac{[SPM] \times [Li]_{sed}}{[SPM] \times [Li]_{sed} + [Li]_{diss}} \times 100 \quad (1)$$

with [SPM] being the concentration of suspended sediments (in g/L), $[Li]_{sed}$ and $[Li]_{diss}$ the Li concentration in sediments (in ppm) and water (in ppb) from Dellinger et al. (2014) and Tables (1 and 2). Here we use the long-term average of sediment fluxes derived from both sediment gauging (Meade et al., 1979; Guyot et al., 1996; Wittmann et al., 2011) and comogenic nuclides (Wittmann et al., 2011) when available (values are reported in Table S1) rather than the instantaneous sediment flux measured the day of the sampling because daily SPM concentration can vary over three orders of magnitude depending on the hydrological stage (*e.g.* Armijos et al., 2013). Between $\sim$ 40 and 97% of Li is transported in the solid form in the Amazon rivers (Fig. 4). For most of the river samples, this proportion is higher than 95%. The lowland rivers, especially those draining the shields have the highest proportion of Li transported in the dissolved load, (e.g. Tapajós and Trombetas rivers). This difference between lowland and Andean rivers is consistent with the results for the Orinoco River (Huh et al., 2001). It should be noted that this calculation does not take into account the variability in $[Li]_{sed}$ with depth and especially the decrease of Li concentration in suspended sediments toward the bottom of the river due to the dilution with quartz minerals (Dellinger et al., 2014). The predominant form of Li transported in the Amazon River basin is thus the solid phase in agreement with what was found at the global scale (Misra and Froelich, 2012; Li and West, 2014).

5.2. Source of dissolved lithium

In the Amazon basin, potential sources of dissolved Li include rainwater, dissolution of evaporites, carbonates and silicates. As Li is not a nutrient, vegetation is not expected to be a significant sink or source of Li. In the following we estimate the proportion of Li deriving from each source and demonstrate that dissolved Li in Amazon rivers is mostly sourced from silicate weathering.

5.2.1. Atmospheric inputs

Only few data on Li concentration and isotope composition of rainwater have been reported so far (Pistiner and Henderson, 2003; Pogge von Strandmann et al., 2006, 2010; Lemarchand et al., 2010; Millot et al., 2010a). These studies have shown that Li in rainwater derives from both marine aerosol and silicate mineral dust. Following Gaillardet et al. (1997), we assume that dust-derived trace elements in rainwater are sourced from the Amazon Basin itself and perform a correction only for marine aerosols using the characteristics of modern seawater. The seawater Li/Cl ratio is on average equal to 5.10^{-5} (Millot et al., 2010c) and its δ^7Li = +31‰ (Millot et al., 2007). The concentration of the element X deriving from atmospheric input is :

$$[X]_{rain} = [Cl]_{rain} \times \left(\frac{X}{Cl}\right)_{ocean} \quad (2)$$

The maximum estimated chlorine concentration deriving from marine inputs ($[Cl]_{rain}$) has been assumed to be 20 μmol.L^{-1} for large Amazon tributaries (Gaillardet et al., 1997) and 3 to 8 μmol.L^{-1} for the eastern river basins in Bolivia, Peru and Ecuador (Stallard and Edmond, 1981; Moquet et al., 2011). The calculated $[Li]_{rain}$ is low, with a maximum estimated contribution of rainwater-derived Li of $\sim$ 2% for the shield rivers, 0.5-1% for the main tributaries (Solimões, Madeira and Amazon at Obidos) and less than 0.1% for Andean rivers. The dissolved δ^7Li is therefore not corrected for atmospheric input because the estimated shift of Li isotope composition associated with this marine contribution is less than 0.3‰ which we consider as a very minor.

5.2.2. Evaporites

Some rivers have Cl concentrations exceeding $[Cl]_{rain}$, which suggests that they are influenced by halite dissolution. Marine evaporites deposits have been reported (salt domes) essentially in the Ucayali and Marañón basins (Huallaga River). Chlorine concentration derived from evaporite dissolution is estimated by subtracting $[Cl]_{rain}$ to the river Cl concentration ($[Cl]_{ev}$ = $[Cl]_{diss}$ - $[Cl]_{rain}$), and the concentration of Li derived from halite dissolution is :

$$[Li]_{ev} = [Cl]_{ev} \times \left(\frac{Li}{Na}\right)_{ev} \quad (3)$$

Assuming congruent dissolution of halite and using a mean Li/Na value of 3×10^{-5} for marine evaporites (Reeder et al., 1972; Kloppmann et al., 2001; Imahashi et al., 1993), we calculate a maximum contribution of Li deriving from evaporite dissolution of 11% for the Huallaga River and less than 1% for most of the other rivers. The contribution of evaporites to the dissolved Li load is thus relatively minor. In the following, the concentration of the element X corrected from rainwater and evaporite input is referred to [X]* ($[X]^* = [X]_{diss} - [X]_{rain} - [X]_{ev}$).

5.2.3. Carbonates and silicates

Several studies on rivers draining mixed lithologies show that the input of Li from the weathering of carbonates is generally negligible compared to silicate weathering inputs (Kisakurek et al., 2005; Millot et al., 2010c). Following Millot et al. (2010c), we can use the typical Li/Ca molar ratio in carbonates ($\sim 1.5 \pm 0.5 \times 10^{-5}$) (Hathorne and James, 2006; Pogge von Strandmann et al., 2013), and by assuming that all the dissolved calcium derives from carbonate weathering, estimate the maximum proportion of Li deriving from carbonate weathering.

$$[\mathrm{Li}]_{\mathrm{carb}} = [\mathrm{Ca}]^* \times \left(\frac{\mathrm{Li}}{\mathrm{Ca}}\right)_{\mathrm{carb}} \quad (4)$$

Altogether, our calculation shows that more than 95% of the dissolved Li is derived from silicate weathering, confirming the previous studies on large river basins with mixed lithologies and the negligible input of Li from carbonate weathering (Huh et al., 2001; Kisakurek et al., 2005; Millot et al., 2010c). Therefore, it is not necessary to correct the $\delta^7\mathrm{Li}_{\mathrm{diss}}$ from non-silicated sources.

5.3. Lithium isotope fractionation during continental weathering

The dissolved load of the Amazon rivers is strongly fractionated toward high δ^7Li values compared to the source rock (Fig. 2). This result is entirely consistent with Dellinger et al. (2014) who showed that the δ^7Li values of river sands from Amazon rivers cover a range comparable to that of bedrocks while suspended sediments are slightly enriched in ^{6}Li. Dissolved load and suspended load appear thus to be complementary reservoirs (Fig. 2). As none of the various non-silicates sources (rain, evaporites, carbonates), nor the δ^7Li variability in the silicate bedrock can account for the range of dissolved δ^7Li, we concluded that most of the fractionation of Li isotopes is produced by silicate weathering processes and sorting, consistently with previous studies on small and large basins (Huh et al., 1998; Pogge von Strandmann et al., 2006; Vigier et al., 2009; Millot et al., 2010c).

5.3.1. Evidence for Li incorporation in secondary minerals

Both experimental and field-based studies (*e.g.* Huh et al., 1998; Pistiner and Henderson, 2003; Vigier et al., 2008; Verney-Carron et al., 2011) have shown that incorporation or adsorption of Li into secondary weathering products (clays and iron hydroxides) is accompanied by large Li isotope fractionation. According to Millot et al. (2010c), the Li incorporation into secondary minerals can be revealed by comparing the concentration of Li with an element that is much less sensitive to this process (a conservative element) such as Na or Mg. Indeed, both Na and Mg are most likely released in solution at the same rate as Li during mineral dissolution (Verney-Carron et al., 2011). Yet, unlike Li which has a strong affinity for clay minerals and oxyhydroxides, Na and Mg are in most cases not significantly incorporated into secondary weathering products (Sawhney, 1972) We note however that significant incorporation or adsorption of Mg can occur (depending of the clay mineral phase) as indicated by studies on Mg isotopes (Tipper et al., 2006, 2012; Huang et al., 2012; Wimpenny et al., 2014, e.g.,). Another complication for the use of Mg is the influence or carbonates. These issue are addressed in the appendix A.

The $\delta^7\mathrm{Li}_{\mathrm{diss}}$ of Amazon rivers is negatively correlated with the dissolved $(\mathrm{Li/Na})^*$ and $(\mathrm{Li/Mg})^*$ (Fig. 5). The most Li-depleted rivers (relative to Na and Mg) have the highest δ^7Li values, and vice-versa. The correlation between $(\mathrm{Li/Na})^*$ and $\delta^7\mathrm{Li}_{\mathrm{diss}}$ is weaker than that with $(\mathrm{Li/Mg})^*$, with the rivers draining the shield being shifted toward lower $(\mathrm{Li/Na})^*$ values compared to other rivers. These correlations suggest that in the Amazon basin, Li isotope fractionation in the dissolved load is linked to Li incorporation in solid weathering products. Whether Li in secondary minerals is incorporated into the mineral structure or is adsorbed at the mineral surface cannot be further constrained with the present dataset and in the following we do not distinguish between these two processes. Following Gislason et al. (1996), Georg et al. (2007) and Millot et al. (2010c), the proportion of Li initially dissolved remaining in solution after secondary mineral formation ($f^{\mathrm{Li}}_{\mathrm{diss}}$), can be calculated as :

$$f^{\mathrm{Li}}_{\mathrm{diss}} = \frac{(\mathrm{Li/X})_{\mathrm{diss}}}{(\mathrm{Li/X})_0} \quad (5)$$

Where X is Na or Mg and $(Li/X)_0$ corresponds to the initially dissolved Li/X ratio before incorporation of Li in secondary minerals. A f^{Li}_{diss} value of 1 means that Li is not re-incorporated in secondary minerals after its initial dissolution (congruent dissolution) while a value of 0 indicates that all the lithium initially dissolved has been re-incorporated into secondary weathering products. Within the assumption that Li, Na and Mg are congruently dissolved from the rock sources, the $(Li/X)_0$ ratio can be calculated by the following equation :

$$\left(\frac{Li}{X}\right)_0 = \sum_i \left(\frac{Li}{X}\right)_i^{rock} \gamma_i^X \quad (6)$$

Where γ_i^X are the mixing proportions of the element X of each rock source i contributing to the dissolved load and $(Li/X)_i^{rock}$ are the (Li/X) ratio of each rock source i. In the Amazon basin, estimation of the $(Li/X)_0$ values is critical because the range of Li/Na and Li/Mg values in the silicate source rocks and river sands is very large and could at least partly explain the scatter of river data (Fig. 5). Shales are Li-rich (60-80 ppm) compared to granitic rocks (10-45 ppm) and volcanic rocks (5-20 ppm) (Holland, 1984; Teng et al., 2008; Burton and Vigier, 2011). In the next section, we discuss the different methods used to correct for source rock variability and calculate the $(Li/X)_0$ ratio for each river.

5.3.2. Determination of the $(Li/X)_0$ ratio of each river basin

For the Madeira and Solimões rivers, we use the riverine dissolved strontium isotope composition ($^{87}Sr/^{86}Sr$) to determine the $(Li/X)_0$ of each river. Sr isotope have been extensively used as a source tracer in rivers (e.g. Palmer and Edmond, 1992) because (i) Sr is generally conservative in river water and (ii) the $^{87}Sr/^{86}Sr$ ratio is "insensitive" to weathering processes (dissolution and precipitation of new mineral phases). In the Amazon basin, the silicate source rock comprises both igneous (mostly andesites and granodiorites) and sedimentary rocks (Stallard and Edmond, 1983) that have distinct $^{87}Sr/^{86}Sr$ ratio values (Petford and Atherton, 1996; Roddaz et al., 2005; Bryant et al., 2006). The $(Sr/Na)^*$ and $(^{87}Sr/^{86}Sr)^*$ ratios of the rivers of the Madeira basin can be explained by a mixture between carbonate and shale weathering (Fig. 6), which is consistent with the geology of the Madeira Basin composed exclusively of sedimentary rocks. Rivers of the Solimões basin plot closer to the igneous rocks - carbonates mixing line, with a variable contribution of shale weathering (Fig. 6). This is again in good agreement with the lithology of those basins where both sedimentary and igneous rocks are present in the bedrock. Collectively, it shows that the respective input of shales and igneous rock weathering to the dissolved load can be estimated using the dissolved $^{87}Sr/^{86}Sr$. A mixing model between five end-members (atmospheric, evaporite, shale, igneous rocks and carbonate) can be solved using an inverse method in order to determine, for each river, the contribution of the different sources (Gaillardet et al., 1997). The determination of the compositional range of each end-member, as well as the mixing proportion of Na (γ_i^{Na}) are detailed in appendix A.

Results of the mixing model show that in the Madeira basin, the contribution of igneous rock weathering is negligible (except in the Orthon River), consistently with the scarcity of igneous rocks in the Madeira watershed. In the Solimões basin, we find that Na_{sil} (i.e. dissolved Na deriving from silicate weathering) is mostly sourced from igneous rocks weathering for the Morona, Pastaza and Maranon at Borja ($> 70\%$), while essentially derived from shale weathering for others tributaries (> 50 to 80%). Using Eq. (12) with the mixing proportions (γ_i^{Na}) and the mean Li/Na ratio of the source rocks, we calculate the $(Li/Na)_0$ for each river (see Appendix B).

For the rivers draining the Brazilian and Guiana shields, the source rock corresponds essentially to shield

rocks which have a granodioritic composition similar to Upper Continental Crust (UCC) (Gaillardet et al., 1997). Because the $^{87}Sr/^{86}Sr$ ratio of shield rocks is similar to that of shales, the $^{87}Sr/^{86}Sr$ cannot be used to calculate the respective contribution of granitic and shale rocks weathering and estimate the $(Li/X)_0$ of shield rivers. We rather use the trends between δ^7Li, (Li/Mg) and (Li/Na) defined by shield rivers in Fig. (5) to estimate the $(Li/X)_0$ of shield rivers (see Appendix B).

5.3.3. Calculation of the f^{Li}_{diss} values and covariation with δ^7Li

With the $(Li/X)_0$ of each river estimated in the previous section, it is possible using Eq. (5) to calculate the f^{Li}_{diss} value for the different rivers (Table 3). For the Madeira and Solimões river basins, the f_{Li} are calculated using only Na and not Mg in Eq. (5) because in those basin, a large part of the Mg is derived from carbonate weathering. For the rivers draining the Brazilian and Guiana shields, f^{Li}_{diss} are calculated using both Na and Mg because (i) the contribution of carbonate weathering is low (Gaillardet et al., 1997), or negligible (Edmond et al., 1995) and (ii) [Na]* concentrations are very dilute and have a larger uncertainty than $[Mg]_{diss}$* (see Appendix B for more details).

In the Madeira basin, the calculated f_{Li} values range from as low as 0.04 for the Mamore River to 0.69 in the Challana River (Table 3). In the Solimões River basin, the f^{Li}_{diss} values range from 0.06 in the Huallaga River to 0.32 in the Ucayali River (Table 3). Finally, in the rivers draining the Amazonian shield, f^{Li}_{diss} range from 0.17 for the Jaciparana River to 0.80 in the Negro River. No systematic variation of f^{Li}_{diss} with the geomorphic and weathering regime is observed. The Beni River tributaries characterized by a "weathering-limited" regime (Moquet et al., 2011; Bouchez et al., 2014) display the same range of f^{Li}_{diss} variation than "supply-limited" rivers draining the Amazonian plain and shield areas. These values are high indicating little net Li re-incoporation. The main tributaries of the Madeira River basin are characterized by a high proportion of Li incorporated into secondary minerals ($f_{Li} < 0.20$), with the Mamore River having the lowest f^{Li}_{diss} from all rivers studied here. In the Beni River basin, the variability of the f^{Li}_{diss} values is also very large. The rivers draining the Eastern Cordillera with the highest relief (Tipuani, Challana, Mapiri, Coroico) have generally lower f^{Li}_{diss} values than the rivers of the subandean zone (Alto Beni, Chepete and Quiquibey) indicating more net Li incorporation in the Andean zones with low relief.

By combining the mixing proportion of sodium (γ^{Na}_i) and the (Li/Na) ratio of the source rocks, it is possible to calculate the proportion of dissolved Li initially released in solution (before incorporation in secondary minerals) from the various sources (Table 3). Because shales are enriched in Li compared to igneous rocks, we find that in the Solimões River basin, the maximum proportion of Li initially dissolved from igneous rocks is only 20% (for the Morona and Pastaza rivers) despite the fact that the majority of the sodium in these rivers derives from the weathering of igneous rock. This shows that even in catchments dominantly underlain by igneous rocks, most of the lithium derives from the dissolution of silicate sedimentary rocks. In the Amazon basin, weathering of silicate sedimentary rocks exerts a significant control on the dissolved Li flux.

Overall, the δ^7Li_{diss} values are well correlated to f^{Li}_{diss} at the scale of the whole Amazon River basin (Fig. 7). The rivers that have the lowest proportion of Li incorporated into secondary minerals ($f^{Li}_{diss} > 0.6$ for the Challana, Tipuani and Negro rivers) also have the lowest Li isotope composition while the highest δ^7Li_{diss} values are associated with high proportion of Li incorporated into the solid ($f^{Li}_{diss} < 0.1$). This demonstrates unambiguously that the first-order control on the δ^7Li_{diss} in the Amazon basin is the proportion of Li incorporated in present-day products of silicate weathering. The comparison between Fig. (5) and Fig. (7) also emphasises the importance of considering source rock variability to quantify Li incorporation in

secondary minerals. An interesting observation is that major tributaries of the Madeira and Solimões rivers (green and red squares in Fig. 7) all lie above (higher δ^7Li_{diss}) the trend defined by the Andean, clear and black waters in Fig. (7) although their waters are a mixture of waters from these different zones. This, in particular, shows that the δ^7Li_{diss} of main tributaries of Madeira and Solimões basins cannot be explained only by the mixing of lowland and Andean tributaries. In other words, either the δ^7Li is not conservative or a Li source is missing (see section 6.3 for further discussion).

5.4. Modeling the Li isotope fractionation during Li incorporation in secondary minerals

5.4.1. Dissolved load

To assess the influence of the weathering regime on the dissolved δ^7Li, the trends of the Fig. (7) can be modelled using a mass balance model (Johnson et al., 2004; Georg et al., 2007; Bouchez et al., 2013). Such a simple approach allows for the determination of field-based fractionation factors associated with the incorporation of Li into secondary minerals. Conceptually, we first consider the weathering zone as an open flow-through system in which Li is released in a dissolved form by dissolution of primary minerals and removed from solution by incorporation into secondary minerals. At steady state, all dissolution and precipitation input and output fluxes and isotope composition are balanced, and the Li isotope composition can be modelled as (Bouchez et al., 2013) :

$$\delta^7Li_{diss} = \delta^7Li_0 - \Delta_{sec-diss} \times (1 - f_{Li}) \tag{7}$$

$$\delta^7Li_{sec} = \Delta_{sec-diss} + \delta^7Li_{diss} \tag{8}$$

Where δ^7Li_0, δ^7Li_{diss} and δ^7Li_{sec} correspond to the Li isotope composition of the initial solution after dissolution, the dissolved load and the solid weathering products, respectively. With no fractionation during dissolution (Pistiner and Henderson, 2003), the term δ^7Li_0 corresponds to the mean δ^7Li_{rock} of the weathered rocks. The term $\Delta_{sec-diss}$ is the isotope fractionation factor between secondary products and the dissolved load ($\Delta_{sec-diss} = \delta^7Li_{sec} - \delta^7Li_{diss} = 1000\ \ln(\alpha_{sec-diss})$). The assumptions behind this steady-state model are extensively discussed in Bouchez et al. (2013). Large river systems have the advantage to integrate the spatial variability in isotope signatures and processes, and to "smooth" the temporal variability, such that the assumption of steady-state is most valid at this scale For the sake of simplicity in the following we refer to this mass balance model as the "batch" system although it should be emphasized that the mass transfer underlying this model is different from that of a true batch model.

Another fractionation model is the Rayleigh distillation model, where secondary products do not re-dissolve. In this model, the isotope composition of the dissolved load can evolve toward higher Li isotope composition than in the batch model.

$$\delta^7Li_{diss} = \delta^7Li_0 + \Delta_{sec-diss} \times \ln(f_{Li}) \tag{9}$$

The exceptionally large range of f^{Li}_{diss} values in the Amazon rivers allows us to discriminate between these two models. At first order, both models are able to explain the variability in δ^7Li_{diss} of Amazon basin rivers (Fig. 7). However, the data are better explained by two separate trends : (i) a "batch" fractionation curve for the Beni Andean rivers, lowlands rivers and shield tributaries and (ii) a Rayleigh distillation curve for the main tributaries of Madeira and Solimões basins. This difference of fractionation behaviours have

also been reported for the silicon isotopes in Iceland (Georg et al., 2007) and in the Amazon (Hughes et al., 2013).

For the first set of rivers, the linear trend (Fig. 7) shows that as a whole, each river basin can be reasonably described as a single "batch" reactor (Eq. 7) with its own characteristic $f^{\mathrm{Li}}_{\mathrm{diss}}$ value. Therefore, the variability in $\delta^7\mathrm{Li}_{\mathrm{diss}}$ across these rivers stems from a similar process (same $\alpha_{\mathrm{sec-diss}}$) and type of mass exchange between compartments ("batch" model), but characterised by a different extent of reaction ($f^{\mathrm{Li}}_{\mathrm{diss}}$). A linear trend as observed in Fig. (7) does not result from a mixture between end members (such mixing trend would be an hyperbola).

The slope of the correlation (Fig. 7) yields a fractionation factor between dissolved and secondary products $\alpha_{\mathrm{sec-diss}} = 0.983 \pm 0.002$ (n = 22, $r^2 = 0.86$), or $\Delta_{\mathrm{sec-diss}}$ = -17‰. This fractionation factor value is in very good agreement with experimental data (precipitation of smectite and basalt alteration phases at various temperatures) (Vigier et al., 2008; Millot et al., 2010b) and the global Li isotope fractionation trend compiled by Li and West (2014). We also note that a single fractionation factor is needed to explain the data of Andean, lowlands and shield rivers. This means that the fractionation factor is independent of the type of the secondary minerals phases as lowland and shield rivers transport high amounts of kaolinite and smectite whereas the Andean rivers sediments clay-sized are mostly composed by an illite-chlorite clay assemblage (Guyot et al., 2007). This observation is in good agreement with recent experimental data (Vigier et al., 2011).

The second set of rivers define a specific Rayleigh trend with a fractionation factor $\alpha_{\mathrm{sec-dis}}$ of 0.991 ± 0.002. The two different isotope fractionation factors suggest that different processes generate Li isotope fractionation in the Andes/shield and along the course of the Madeira River. Furthermore, the fact that the data along the Madeira and Solimões large tributaries are better fitted by a different mass balance model would suggest that the way water and sediments interact is different there from the rest of the basin (see section 6.3). However, unlike the rivers fitting the batch fractionation model, the Solimões and Madeira main tributaries Li isotope composition and $f^{\mathrm{Li}}_{\mathrm{diss}}$ variability could also be explained by a mixing trend between two end members (for example, between two end members having signature of the Mamore and Beni rivers). This issue is addressed in the section 6.3 of this paper.

5.4.2. Suspended load

The δ^7Li of the suspended load can be used to test the batch fractionation model previously defined. For simplicity, we focus only on rivers fitting the batch fractionation model. Using the fractionation factor ($\alpha_{\mathrm{sec-diss}}$) previously determined from the dissolved load, we can predict the δ^7Li of the modern-day weathering products (clays and oxides) using Eq. (8) and compare them to the δ^7Li measured in the suspended loads (Fig. 8). For a given fractionation factor, Eq. (8) predicts that $\delta^7\mathrm{Li}_{\mathrm{sec}} - \delta^7\mathrm{Li}_{\mathrm{rock}}$ is linearly related to f_{Li}. In this study and for most of the rivers, only surface sediments have been sampled and thus are plotted in Fig (8) although a large variability of sediment Li concentration and isotope composition with depth has been reported (Dellinger et al., 2014).

Two different trends can be identified in Fig. (8). The first one corresponds to the lowland and shield rivers (except for the Rio Negro). In these rivers, the δ^7Li of surface sediments plot within uncertainty on the predicted isotope composition of modern weathering products and are therefore in good agreement with the fractionation factor ($\alpha_{\mathrm{sec-diss}}$) and $f^{\mathrm{Li}}_{\mathrm{diss}}$ values deduced from the study of the dissolved load. This is consistent with a supply-limited weathering regime where SPM is formed of secondary weathering products because primary minerals are completely weathered before being transported away from the weathering zone

(West et al., 2005). For Andean rivers, surface sediment δ^7Li is systematically higher than the expected value for secondary minerals. Two hypotheses can explain this discrepancy (i) the batch fractionation model does not satisfactorily explain those data or (ii) the suspended sediments of Andean rivers is not composed only by the complementary phase of the dissolved load but also contains an unweathered rock component having Li isotope composition similar to that of shales. This conclusion is in perfect agreement with Dellinger et al. (2014) that showed that in the Andean rivers, the proportion of unweathered bedrock fragments in the suspended load of these rivers can reach 70 %.

Finally, although it could be expected that the Rio Negro transports only secondary weathering products, its sediment δ^7Li is different from δ^7Li_{sec} predicted by Eq. (8). The Negro River is characterized by very high f^{Li}_{diss} values, indicating that the proportion of Li incorporated into secondary minerals is rather small compared to other rivers. Therefore even very small amounts of unweathered sediments transported by the Rio Negro could significantly increase the δ^7Li of its sediments. This result would be in good agreement with mineralogical data showing that the Rio Negro suspended load contains only 10 to 20% clay minerals, with the remaining being quartz minerals and organic colloids (Brinkmann, 1986). However, we cannot exclude that the high δ^7Li_{sed} of the Rio Negro is influenced by atmospheric dusts having higher Li isotope composition than secondary clays.

6. What controls the incorporation of Li in secondary phases and the dissolved Li isotope composition ?

As shown above, δ^7Li_{diss} is controlled by the proportion of Li incorporated into secondary minerals. In this section we discuss the parameters which control the proportion of Li incorporated in secondary minerals, and thereby river dissolved δ^7Li.

6.1. Control by denudation rate and residence time in the weathering zone

We focus in this section only on the rivers fitting the "batch" fractionation model in Fig. (9.a), i.e. lowland and Andean rivers. Other rivers (main tributaries of the Madeira and Solimoes rivers) will be discussed separately in the section 6.3. Fluid flow (e.g. Maher and Chamberlain, 2014; Wanner et al., 2014) and mineral residence time (Ferrier and Kirchner, 2008; Bouchez et al., 2013) are two main controls on the transfer of elements during weathering. We explore here the links between δ^7Li_{diss}, the dissolved flux of Li and the denudation rate, as proposed by Bouchez et al. (2013). The total denudation rate (D) used here corresponds to the sum of the silicate chemical weathering rate (as defined by Bouchez and Gaillardet, 2014) and physical denudation rate. Total denudation rates are based on either long-term sediment and solute data (Guyot et al., 1996; Laraque et al., 2009; Filizola and Guyot, 2009; Mortatti and Probst, 2003; Moquet et al., 2011) or from cosmogenic nuclide concentrations in river sands (Safran et al., 2005; Wittmann et al., 2009, 2011).

At first order, the dissolved Li flux of the different river basins is positively correlated ($r^2 = 0.84$) to both sediment gauging and cosmogenic-nuclide derived denudation rates (Fig. 9.c), while showing only a weak correlation to the silicate weathering rate ($r^2 = 0.37$) and no global correlation with runoff. Rivers having the highest denudation rates (Beni rivers) have the highest Li fluxes while the shield rivers have the lowest dissolved Li flux. This correlation reflects the first-order control on the dissolved Li flux by denudation and show that mineral residence time rather that fluid residence time controls the dissolved Li flux in the Amazon basin.

In the Andes, high denudation rates prevail, which lead to short residence times of solid in soils and rivers. Under these conditions, weathering regime is said to be "weathering-limited". The δ^7Li of rivers draining the Bolivian Andes defines a negative correlation with cosmogenic nuclide-derived denudation rates, on which also fit the lowland "clear water" rivers (Fig. 9.a). On one hand, the Challana River, which has the lowest δ^7Li among Andean rivers, also has the highest cosmogenic denudation rate. At the other end, the Tapajós and Orthon rivers have very low denudation rates and high δ^7Li value. A similar correlation has also been recently observed by Pogge von Strandmann and Henderson (2015) for rivers in New Zealand. As suggested by Bouchez et al. (2013) on the basis of the model of Ferrier and Kirchner (2008), this correlation can be attributed to the kinetic limitation (resulting from high erosion rates) on secondary products precipitation. Very high erosion rates limit the formation of soils and the precipitation of clay minerals (high $f^{\mathrm{Li}}_{\mathrm{diss}}$, Fig. 9.b) as the residence time of solids at the Earth surface is too short (Bouchez et al., 2013). If the kinetics of clay mineral precipitation is too slow compared to the rate of sediment export within the basin, only small amounts of Li will be incorporated into secondary minerals (Fig. 9.B). As a result, weathering will appear to be congruent with $\delta^7\mathrm{Li}_{\mathrm{diss}} \approx \delta^7\mathrm{Li}_{\mathrm{rock}}$. At lower denudation rates (< 100 t.km^{-2}.y^{-1}), particle residence time becomes longer and mineral precipitation take place, leading to higher $f^{\mathrm{Li}}_{\mathrm{diss}}$ and hence Li isotope fractionation with $\delta^7\mathrm{Li}_{\mathrm{diss}} > \delta^7\mathrm{Li}_{\mathrm{rock}}$. It is worth noting that the correlation between δ^7Li and the sediment gauging derived denudation rate is less significant than the cosmogenic nuclide derived denudation rate, although the rivers having the highest "sediment gauging derived" denudation rates (except the Alto Beni river) have generally lower δ^7Li than lowland "clear waters". This could indicate that the Li isotopes reflect processes occurring on the millennium time scale (corresponding to the cosmogenic-derived denudation rate) rather than on the decadal time scale. In this regard, the fact that the Alto Beni river does not plot on the correlation defined by other rivers might be due to the recent mobilization of Plio-Quaternary sediments (Dosseto et al., 2006b) resulting in much higher short-term denudation rates than the long-term average.

At very low denudation rate, some rivers (Trombetas and Rio Negro rivers) also have very low δ^7Li values (Fig. 9.a). Indeed, at these low denudation rates, clays reside in the weathering zone for a very long time (Mathieu et al., 1995; Dosseto et al., 2006a) and may be re-dissolved which hence results in "congruent weathering" conditions (Misra and Froelich, 2012; Froelich and Misra, 2014; Ryu et al., 2014) in a way that there is no export of isotopically fractionated Li in the solid load (Bouchez et al., 2013). The variability of the δ^7Li values of these rivers is explored in the next section. In summary, for rivers fitting the "batch" fractionation model, both very high and very low denudation rates produce congruent weathering and similar Li isotope composition.

6.2. Supply-limited weathering regime in the lowlands

Lowland areas are characterized by a "supply-limited" or ("transport-limited") weathering regime (Stallard and Edmond, 1983), with some river waters having low pH and high dissolved Al, Fe and organic matter concentrations. In such environments, organic acids enhance dissolution rates and weathering intensity of silicates (Viers et al., 1997, 2000). The DOC (Dissolved Organic Carbon) concentrations were not measured on those samples so we use the dissolved Al concentration as a proxy for the DOC concentrations. Indeed, in those rivers, the dissolved Al content and pH are controlled by the amount of dissolved organic matter (Viers et al., 1997; Deberdt et al., 2002). The dissolved δ^7Li of shield rivers is well correlated to both the dissolved Al/Li ratio and pH (Fig. 10). The most Al-depleted rivers correspond to the "clear water" rivers and have relatively high δ^7Li compositions while the most Al-rich rivers have low pH values and δ^7Li, and correspond to the "black water" rivers like the Negro River.

The "clear water" rivers (e.g. Tapajós River) contain lower levels of dissolved organic carbon and drain lateritic soils, rich in kaolinite and iron-oxides, and developed on the shield and tertiary sediments (Stallard and Edmond, 1983; Fritsch et al., 2011). In such environments, the formation of kaolinite during present-day dissolution-precipitation processes results in a limited loss of Al and Fe compared to Si (Fritsch et al., 2011). We suggest, similarly to the study of Ryu et al. (2014) that Li is also retained in the solid residue, and that this process drives the δ^7Li_{diss} toward heavy values as a result of isotope fractionation during the formation of kaolinite and iron oxide. On the opposite, the "black waters" such as the Negro River are associated with acidic and reducing waterlogged podzolic soils where dissolution of iron oxides and clay minerals predominate compared to precipitation reactions (Fritsch et al., 2011). Those soils are clay-depleted and dominated by coarse quartz minerals (Brinkmann, 1986; Do Nascimento et al., 2004), where water is well-drained. This results in a net export of aluminium and iron to the river waters through the formation of organo-metallic complexes (Allard et al., 2011; Fritsch et al., 2011). As a result we suggest that in these areas, there is the net dissolution of ^{7}Li-depleted secondary minerals (near the surface of the weathering profile) along with the net formation of secondary minerals (at depth). If both reactions occur at the same rate (i.e. steady-state), rock-like dissolved δ^7Li are obtained in water draining the profile. Podzolisation in the Amazon basin occurs in flat and swampy areas where organic matter accumulate. There is thus an indirect control between topography and Li isotope composition in the plains of the Amazon basin. Such interpretation is in good agreement with the conclusions of Hughes et al. (2013) on the Si isotope composition of the Rio Negro. Furthermore, the correlation of the δ^7Li with dissolved Al content is very similar to that described by Cardinal et al. (2010) for silicon isotopes in the Congo River basin and is interpreted in the same manner.

To summarize, the lowlands are characterized by two distinct weathering regimes, as proposed by Bouchez et al. (2013) for low denudation rates setting : (i) lateritisation processes resulting in a high proportion of Li incorporated in secondary minerals ; (ii) podzolisation, where clay minerals previously formed are dissolved by organic matter, equivalent to congruent weathering of the silicate crust and leading to rock-like δ^7Li values. The difference between these two types of weathering regimes is probably related to large contrasts in runoff and topographic features. Other examples of congruent weathering with no fractionation in the dissolved load compared to the bedrock have been reported in some other extreme weathering environments (Cardinal et al., 2010; Ryu et al., 2014). Supply-limited weathering regimes can produce a large range of δ^7Li values depending of the proportion of Li incorporated in secondary products and therefore do not necessarily result in congruent weathering and low dissolved δ^7Li as proposed by Huh et al. (2001) and Misra and Froelich (2012).

6.3. The role of floodplains in setting large rivers δ^7Li

The large tributaries, that are not well described by a "batch" fractionation model in Fig. (7), do not plot on the correlation between denudation rates and δ^7Li. Therefore their isotope composition is not controlled only by the mineral residence time in the soil weathering zone and another mechanism must be considered. These main tributaries of the Madeira and Solimões (draining both the Andes and the lowlands areas) at lowland locations have the highest δ^7Li signatures with a proportion of Li incorporated in secondary minerals of more than 80-90%. The δ^7Li of the Beni river increases from 8-12‰ at the outlet of the Andes to 16‰ at the lowland location. This is unexpected because (i) the contribution of dissolved matter from the lowland is small compared to that from the Andes (Gaillardet et al., 1997; Moquet et al., 2011) and (ii) the pure lowland rivers from the Madeira basin have lower δ^7Li values (11.5 to 15.5‰) than the Beni sampled in the lowland. Accordingly, the main tributaries of Madeira and Solimões basins either follow (a) a Rayleigh

mass-balance with a fractionation factor of -9‰, or (b) plot on a mixing trend between an end member having a high f^{Li}_{diss} and a low δ^7Li and another end member having a low f^{Li}_{diss} and a high δ^7Li (Section 5.4.1). These two observations are consistent, with respectively either (a) a process of Li removal associated with isotope fractionation during transfer through the floodplains or (b) an addition of high dissolved δ^7Li source from floodplains areas in the main tributaries. Such influence of floodplains on the dissolved δ^7Li has also been proposed by Pogge von Strandmann and Henderson (2015) to explain the high δ^7Li of eastern rivers from New Zealand.

These two hypotheses can be tested by comparing the net dissolved lithium fluxes transported by the river systems upstream and downstream the floodplain reaches. Such comparison is difficult because only the Andean dissolved Li flux for the Beni river basin is known. However, a first-order estimate of the Andean dissolved Li flux can be determined for each river by multiplying the Li/Na ratio by the dissolved Na flux both derived from the Andes. For this we assume that the f^{Li}_{diss} value of Andean rivers is the same as for the Beni River upstream the floodplain, ranging between 0.2 and 0.4, and we use the mean annual dissolved Na flux deriving from the weathering of silicate rocks from the study of Moquet et al. (2011). This calculation shows that for the main tributaries there is no increase of the net Li flux downstream but rather a decrease, especially for the Mamoré and Huallaga rivers. These two rivers have the highest dissolved Li isotope composition at their mouth.

Another approach is to use the correlation between the denudation rate and the dissolved Li flux (Fig. 9c). At first order, the dissolved Li flux is related to the denudation rate as described in the section 6.1. However, as lowland reaches have low denudation rate, if there is an additional process of supply or removal of dissolved Li in the floodplain, the dissolved Li flux of the main tributaries should be offset (as observed for the Mamore and Huallaga River) compared to the global trend defined by the lowland and Andean rivers. Interestingly, on this figure, the Mamore and Huallaga rivers (that have the highest δ^7Li) are slightly offset compared to the global correlation. Using the equation of the correlation of the Fig. (9c), it is possible to calculate the theoretical dissolved Li flux of the main tributaries and compare it with the actual measured flux as shown on the Fig. (11). On this figure, addition of high δ^7Li lithium in the floodplain should result in a positive correlation. On the contrary, removal of dissolved Li should produce a negative correlation. We observe that all the main tributaries, except the Ucayali river, plot on the negative trend showing that the Amazon floodplain seems to act as a net sink of dissolved Li. This suggest a process-related fractionation of Li isotope rather than mixing with additional source of Li, to explain the very high δ^7Li values. This conclusion is consistent with the observation of dissolved silicon removal inferred from changes in Si isotope fractionation in the seasonal floodplains of the Okavango Delta (Frings et al., 2014).

The exact mechanism responsible for Li uptake in the floodplains can only be speculated at this stage but some hypotheses can be discussed. Downstream from the Andes-lowland transition, river sediments and waters from the main channel are temporally stored in alluvial plains (Guyot et al., 1996; Bouchez et al., 2012). In these environments, water and sediments interact and authigenic secondary minerals might form (Frings et al., 2014) and incorporate part of the dissolved Li. Floodplain lakes and groundwater systems isolated from the main channel during a sufficiently long period of time become closed systems, in which Li could evolve along a Rayleigh fractionation path if a significant amount of Li is incorporated into clay minerals or oxides. Water from floodplain lakes and groundwater returning to the main channel during annual high water stage would then contribute to the increase in δ^7Li-signature of the river. Reactive-transport modelling have shown that subsurface residence time of water (Wanner et al., 2014) and small changes in aquifer conditions (Pogge von Strandmann et al., 2014) can strongly influence the Li isotope composition

of groundwater systems. Although there is no clear correlation between runoff and Li isotope fractionation in the Amazon floodplains, it is interesting to note that the Mamore River (having the highest δ^7Li value) is characterized by the lowest runoff and higher weathering intensity among the main tributaries. This may indicate increasing fractionation along the course of the river, as the contact time between the water and the sediment increases as proposed by Wanner et al. (2014), but validation of this hypothesis would require further investigation of the links between fluid travel time and the evolution of the δ^7Li in the floodplain. Altogether, this shows that Li does not behave conservatively in rivers draining both mountain ranges and floodplains. We estimate that for these rivers, 75 to 90% of the Li removal in secondary minerals takes place in the weathering zone uplands and 10 to 25% in the floodplains. For the Mamore and Huallaga Rivers, up to 90% of the dissolved lithium entering the floodplain reaches is removed in solid weathering products in the floodplain (Fig. 11). Therefore, the dissolved flux of Li is significantly reduced by incorporation of Li into secondary products when water travels through in the floodplains.

6.4. Relation between δ^7Li and weathering intensity

In the Amazon basin, "white", "clear" and "black" waters corresponding to very different weathering regime have distinct Li isotope signatures. The Solimões, Madeira and Amazon rivers correspond to the mixture of these 3 types of waters. Thus, we can calculate that the δ^7Li of the Amazon River at its mouth results from the mixture of 76% of Li deriving from the Andes/floodplains (white waters), 15% from the laterite-lowlands (clear waters) and 9% from the podzol (black waters). About 60% of the dissolved Li derived from the Andes is removed from the dissolved load in floodplains.

We found no clear relationship between δ^7Li_{diss}, dissolved Li fluxes and silicate weathering rates or runoff. Rather, the control imposed by denudation rates, floodplain processes and residence time in the weathering zone observed at the scale of the whole Amazon River basin results in an equivocal bell-curved relationship (Fig. 12) between dissolved δ^7Li and the weathering intensity. The latter is defined here as W/D (Bouchez et al., 2014), the ratio between the chemical silicate weathering rates W (as defined by Bouchez and Gaillardet (2014)) and the total denudation rates D. It corresponds to the fraction of material dissolved from a given mass of rock and is similar to the "CDF" (Chemical Depletion Factor, i.e. Riebe et al., 2001), the "CIA" (Chemical Index of Alteration, i.e. Nesbitt and Young, 1982) or element-specific weathering indexes (i.e. Gaillardet et al., 1997). In the Amazon basin, high weathering intensity (W/D $>$ 0.1) which characterize supply-limited weathering regimes produce low values of δ^7Li (1-15‰) and dissolved Li fluxes (Fig. 9). Weathering-limited regimes in the Andes having very low weathering intensity (W/D $<$ 0.01) have also relatively low δ^7Li similar to supply-limited settings (Fig. 12) but much higher dissolved Li fluxes (Fig. 9). Therefore, both high and low weathering intensity produce low δ^7Li values, but at very different Li fluxes. Finally, main tributaries which integrate both highland and lowland area have intermediate weathering intensities (W/D = 0.01-0.10) with high δ^7Li values (14-32‰) due to secondary processes occurring in the floodplains.

Other river systems for which the δ^7Li_{diss}, along with a reliable estimate of both δ^7Li_{rock} and time-integrated W/D data are available (see table S2), also plot on the same bell-curved relationship as the Amazon rivers (Fig. 12). In this regard, apparent contradictory interpretations from past studies (Huh et al., 2001; Vigier et al., 2009; Pogge von Strandmann et al., 2010; Misra and Froelich, 2012; Pogge von Strandmann and Henderson, 2015) can be reconciled by this non-linear relationship between δ^7Li_{diss} and the weathering intensity. Indeed, rivers from Iceland studied by Vigier et al. (2009) have low W/D and plot on the positive trend between δ^7Li_{diss} and W/D whereas rivers from the Orinoco River from Huh et al.

(2001) have intermediate to high W/D (Edmond et al., 1995, 1996), and therefore plot on the negative trend between δ^7Li_{diss} and W/D. We note that Andean rivers from the study of Huh et al. (2001) have been sampled downstream the floodplain, which may explains their very high δ^7Li_{diss} value.

Altogether, these relationships between δ^7Li, dissolved Li flux, weathering intensity and denudation can be used to constrain paleo weathering and erosion conditions from past Li isotope composition records (Hathorne and James, 2006; Misra and Froelich, 2012; Pogge von Strandmann et al., 2013).

7. Conclusions and global implications

The Li isotope composition of the Amazon River dissolved load displays a large range of variation from +1‰ to +32‰, in relation with the geomorphic regime. We show that the partitioning of Li between the dissolved load and solid weathering products (f^{Li}_{diss} values) governs the Li isotope composition of the dissolved load. Congruent release of Li results in rock-like δ^7Li values, while extensive Li incorporation (and associated Li isotope fractionation) in secondary weathering products drives dissolved Li isotope composition toward higher values. We calculate a single isotope fractionation factor $\alpha_{sec-dis}$ associated with secondary mineral precipitation in soils of 0.983 ± 0.002. This isotope fractionation factor value does not depend on the type of secondary minerals formed and is in good agreement with the values from the experimental studies of Vigier et al. (2008) and Millot et al. (2010b).

These conclusions are consistent with previous interpretation of the Li isotope composition in rivers and sedimentary archives (Misra and Froelich, 2012; Bouchez et al., 2013; Li and West, 2014). However, although a seawater record of Li isotope composition can be interpreted in a relatively straightforward way in terms of Li mass balance, we show how its translation in terms of (present or past) weathering regime is equivocal :

- First, in the Amazon Basin, lowland rivers characterized by "supply-" or "transport-limited" regimes do not necessarily show congruent Li release, and hence display a large range of dissolved δ^7Li values (from +1.2 to +16‰). Relatedly, rock-like δ^7Li values are observed at both ends of the weathering regime spectrum, *i.e.* in lowland settings (*e.g.* Negro River) and in high mountain belts (*e.g.* Beni headwaters). This is because these radically different weathering regimes can lead to similar Li mass balance ("congruent weathering") from the perspective of the dissolved load. Therefore, low δ^7Li values in sedimentary archives (as observed for the early Cenozoic ; Misra and Froelich, 2012) can in principle be interpreted as reflecting the predominance of supply-limited regimes or of high-erosion settings. In such cases, additional constraints (*e.g.* geological arguments or other stable isotope systems with different sensitivity along the spectrum of weathering regimes) are needed to distinguish between these two interpretations. We propose here that the dissolved Li flux can also serve for a better reconstruction of past denudation rates (Li and West, 2014) as high Li dissolved fluxes correspond only to high denudation rates.
- Second, dissolved δ^7Li signatures at the outlet of large rivers are influenced by lowland processes that differ drastically from those prevailing on hillslopes of eroding upland areas. Dissolved Li released by weathering reactions in high-erosion settings is significantly retained in floodplains through interaction with solid particles, resulting in Li isotope fractionation. As this process (1) traps a large fraction of the river dissolved Li flux and (2) obeys a Rayleigh mass balance model with a fractionation factor $\alpha_{sec-dis}$ of 0.991, it can drive the residual dissolved δ^7Li toward extremely high values. Therefore, Li isotope composition of large rivers at their mouth, and hence past variations in the ocean δ^7Li, are not simply the conservative mixture of the various tributaries but might well also reflect variations

in the global extent and style of weathering processes affecting Li in river floodplains. The relative influence of hillslope and floodplain processes on the global riverine dissolved δ^7Li and weathering rates in general remains to be quantified, for both present-day conditions and past variations.

Appendix A : the inversion mixing model between rain, evaporites, carbonates, shales and igneous rocks

The inverse mixing model used here is similar to one by Gaillardet et al. (1997) applied to the Amazon Basin. The main difference is that in the Madeira and Solimões tributaries, we consider two silicate end-members (igneous rocks and shales) instead of one as in Gaillardet et al. (1997). For each dissolved species (X) of a river, the following mixing equations are :

$$\left(\frac{\mathrm{X}}{\mathrm{Na}}\right)^{\mathrm{diss}} = \sum_{\mathrm{i}} \left(\frac{\mathrm{X}}{\mathrm{Na}}\right)_{\mathrm{i}}^{\mathrm{diss}} \gamma_{\mathrm{i}}^{\mathrm{Na}} \tag{10}$$

$$\left(\frac{^{87}\mathrm{Sr}}{^{86}\mathrm{Sr}}\right)^{\mathrm{diss}} \left(\frac{\mathrm{Sr}}{\mathrm{Na}}\right)^{\mathrm{diss}} = \sum_{\mathrm{i}} \left(\frac{^{87}\mathrm{Sr}}{^{86}\mathrm{Sr}}\right)_{\mathrm{i}}^{\mathrm{diss}} \left(\frac{\mathrm{Sr}}{\mathrm{Na}}\right)_{\mathrm{i}}^{\mathrm{diss}} \gamma_{\mathrm{i}}^{\mathrm{Na}} \tag{11}$$

with X = Sr, Ca, Mg, HCO_3 ; i = rain, evaporite, shale, igneous rock and carbonate and $\gamma_{\mathrm{i}}^{\mathrm{Na}}$ is the proportion of dissolved sodium deriving from the end-member i. For example, $(\mathrm{Sr/Na})_{\mathrm{sha}}$ is the Sr/Na ratio of water interacting only with shale lithology. The mixing model is solved by an inverse method similar to the one used by Gaillardet et al. (1997). This inverse method requires defining "a priori" values for all parameters and yields "a posteriori" values as a best fit between the model and parameters.

For the rain, carbonate and evaporite end-member, we use the same Na-normalized ratios as Gaillardet et al. (1997) except for $(\mathrm{Sr/Na})_{\mathrm{ev}}$. Indeed, we note that the Huallaga River, which chemistry is dominated by evaporite input (Cl/Na = 1) has a Sr/Na ratio of 1×10^{-3}, lower that the Sr/Na of the evaporite end-member of 3×10^{-3} reported by Gaillardet et al. (1997) and based on salt springs from Stallard and Edmond (1983). Therefore, here we use an intermediate mean $(\mathrm{Sr/Na})_{\mathrm{ev}}$ value of $2 \pm 1 \times 10^{-3}$ to correct for Sr deriving from evaporite dissolution.

The shale weathering end-member can be constrained using the chemical composition of the Challana and Chepete rivers, which only drain shales. We estimate the respective values for the shale end-member from the chemical composition of these two rivers, corrected from atmospheric inputs : $(\mathrm{Ca/Na})_{\mathrm{sha}} = 0.4 \pm 0.2$, $(\mathrm{Mg/Na})_{\mathrm{sha}} = 0.5 \pm 0.3$, $(\mathrm{HCO_3/Na})_{\mathrm{sha}} = 1.5 \pm 1.0$, $(\mathrm{Sr/Na})_{\mathrm{sha}} = 1.5 \pm 0.5$, $(^{87}\mathrm{Sr}/^{86}\mathrm{Sr})_{\mathrm{sha}} = 0.732 \pm 0.005$. The error bar reflects our knowledge of the parameters.

The igneous rocks in the Solimões basin are andesites in the north (Napo, Pastaza and Morona rivers) and both andesites and granodiorites in the south (Maronon, Huallaga and Ucayali). The $^{87}\mathrm{Sr}/^{86}\mathrm{Sr}$ of andesites in Ecuador display a very narrow range of values with a mean value of 0.7042 ± 0.0003 (Bryant et al., 2006). Similarly, the $^{87}\mathrm{Sr}/^{86}\mathrm{Sr}$ of Andean granodiorites (in the Solimões river Basin) has a narrow range of value of 0.7050 ± 0.0005 (Petford and Atherton, 1996). Therefore, we can estimate that the Sr isotope ratio of the igneous rock weathering end-member is $(^{87}\mathrm{Sr}/^{86}\mathrm{Sr})_{\mathrm{ign}} = 0.7050 \pm 0.0005$. Our dataset does not include any river draining only igneous rocks, but the chemical composition of this end-member can be constrained of the Coca River (Santos et al., 2014), which drains predominantly igneous rocks. Its $^{87}\mathrm{Sr}/^{86}\mathrm{Sr}$ is as low as 0.7055 (Santos et al., 2014), lower than any other published data from the Solimões basin (including our dataset) and very close to the value of the $(^{87}\mathrm{Sr}/^{86}\mathrm{Sr})_{\mathrm{ign}}$ end-member. According to Moquet et al. (2011) the contribution of evaporites and carbonate weathering to the Coca River is low but not negligible. Using the

results of Moquet et al. (2011), we can correct the data for the Coca river (Santos et al., 2014) from carbonate and evaporite inputs to estimate the composition of the pure igneous rock end-member : $(Ca/Na)_{ign} = 0.8 \pm 0.3$, $(Mg/Na)_{ign} = 0.3 \pm 0.2$, $(HCO_3/Na)_{ign} = 3.7 \pm 0.7$ and $(Sr/Na)_{ign} = 4.8 \pm 0.6$.

Appendix B : determination of the $(Li/X)_0$ and f^{Li}_{diss} values

The fraction of Li left in solution after secondary solids formation can be calculated using Eq. (5). With the example of sodium, the $(Li/Na)_0$ can be calculated by the following Equation (12) :

$$\left(\frac{Li}{Na}\right)_0 = \sum_i \left(\frac{Li}{Na}\right)_i^{rock} \gamma_i^{Na} \quad (12)$$

Where γ_i^{Na} are the mixing proportions of each source i calculated by the equations (10) and (11) and $(Li/Na)_i^{rock}$ the ratio (Li/Na) of the rock source i.

Na and Mg can both be used as conservative tracers, each of them presenting advantages and caveats. In some contexts Mg can be incorporated significantly in secondary minerals like smectite. In addition, part of the dissolved Mg derives from carbonate weathering (Gaillardet et al., 1997; Moquet et al., 2011) or in the case of some Solimões catchments from the weathering of gypsum (Moquet et al., 2011). Therefore, an additional correction is needed to obtain silicate-derived Mg whereas Na* can be directly used as Na_{sil}. However, Li and Mg are contained in the same primary minerals phases because they have a similar ionic radius, and hence are most likely released stochiometrically into solution (Huh et al., 1998). Moreover, Mg concentrations are weakly influenced by rainwater and evaporite contribution compared to sodium. This can be critical in the case of very dilute waters like in rivers draining Amazonian shield where cyclic sodium correction results in large uncertainties in the determination of Na* (Gaillardet et al., 1997). In this study, we use Li/Na ratios for Anean rivers and both Li/Na and Li/Mg ratios for shield rivers.

Estimation of the $(Li/Na)_0$ ratio in the Madeira and Solimões river basins

In the Madeira river basin, the lithology is uniform and corresponds almost exclusively to Paleozoic (in the Andes) and Tertiary (in the lowlands) sedimentary rocks having a shale-type composition (Stallard and Edmond, 1983; Roddaz et al., 2005). The largest database of Li concentrations in shales is from Ronov et al. (1970). According to Holland (1984) and based on the database of Ronov et al. (1970), the mean Li and sodium ($[Na_2O]$) concentrations of the shales of the Russian Platform are respectively 80 ppm and 0.081% (N $\sim$ 500) so the mean molar Li/Na ratio is 0.040 ± 0.05. This value is similar to the mean chemical composition of the Beni river bed sands (Li/Na = 0.041, n = 3), that integrate the bedrock variability at the scale of the Beni watershed (Dellinger et al., 2014). In the Solimões river basin, igneous rocks contributes significantly to the weathering budget. For the igneous rock end-member, the andesite median Li/Na compiled from the Georoc database (http ://georoc.mpch-mainz.gwdg.de/georoc/ ; Sarbas and Nohl, 2008) is 0.0014 ± 0.0003 ($2\sigma/\sqrt{N}$, N = 1600), and the granodiorite median Li/Na is 0.0049 ± 0.0013 ($2\sigma/\sqrt{N}$, N = 60). Therefore we use an intermediate value of 0.0030 ± 0.0015 for the igneous rock end-member.

Estimation of the $(Li/Na)_0$ and $(Li/Mg)_0$ ratio in the shield river basins

According to Gaillardet et al. (1997), weathering of Brazilian and Guiana shields operate at steady state over a bedrock having a mean chemical composition similar to UCC (Taylor and McLennan, 1985) which has typically the composition of a granodiorite. We can use the correlations defined by the rivers draining

the shield rocks in the Fig. (5) to infer the $(Li/Na)_0$, $(Li/Mg)_0$ and δ^7Li of shield rivers source rocks. The best correlation is obtained for the Li/Mg ratio, uncorrected for carbonate input despite evidence from the inversion of river chemistry that carbonates are contributing to the dissolved load (Gaillardet et al., 1997). However, more recent studies stated that the Mg/Na variability of rivers draining shield rock in tropical area is inherited from bedrock variability rather than due to mixing with Mg deriving from limestone weathering (Viers et al., 2000; Gurumurthy et al., 2012). Therefore, here we consider that all the Mg derives from silicate weathering. In the Fig. (5), the intercept between the river trend and the mixing trend between granodiorites and shales should give the mean composition of the source rocks. We calculate an intercept source rock δ^7Li value of $+1 \pm 1‰$, and a Li/Mg and Li/Na values of 0.014 ± 0.003 and 0.061 ± 0.010 respectively. This intercept has a Li/Mg and Li/Na ratio slightly higher than the mean value for the granodiorite (Fig. 5). We propose that this is due to a slight input of shales weathering as some outcrops of sedimentary rocks has been described in the shield and the Amazon trough (Brinkmann, 1986; Stallard and Edmond, 1983). This corresponds to a input of 5 to 15% of total $(Na)_{sil}$ and $(Mg)_{sil}$ deriving from the weathering of shales. The f^{Li}_{diss} values calculated with sodium ranges from 0.25 to 0.76 and with Mg from 0.16 to 1.00. There is generally less than 20% difference between the two estimate and therefore we use the mean value between the f^{Li}_{diss} determined with Na and Mg.

Acknowledgments

This work was funded by the CNRS-INSU program Syster and the "Réseau des Bassins Versants". Parts of this work were also supported by IPGP multidisciplinary program PARI, and by Paris–IdF region SESAME Grant no. 12015908. We would like to thank Joshua West, Mark Torres, Jotautas Baronas, Friedhelm von Blanckenburg and Julien Moureau for discussions and analytical assistance. This is IPGP contribution XXXX.

References

Aalto, R., Dunne, T., Guyot, J. L., 2006. Geomorphic controls on Andean denudation rates. J. Geol. 114 (1), 85–99.

Allard, T., Weber, T., Bellot, C., Damblans, C., Bardy, M., Bueno, G., Nascimento, N., Fritsch, E., Benedetti, M., 2011. Tracing source and evolution of suspended particles in the rio negro basin (brazil) using chemical species of iron. Chemical Geology 280 (1), 79–88.

Armijos, E., Crave, A., Vauchel, P., Fraizy, P., Santini, W., Moquet, J.-S., Arevalo, N., Carranza, J., Guyot, J.-L., 2013. Suspended sediment dynamics in the amazon river of peru. Journal of South American Earth Sciences 44, 75–84.

Berner, R., 1990. Atmospheric carbon dioxide levels over Phanerozoic time. Science 249 (4975), 1382.

Berner, R., Lasaga, A., Garrels, R., 1983. The carbonate-silicate geochemical cycle and its effect on atmospheric carbon dioxide over the past 100 million years. Am. J. Sci 283 (7), 641–683.

Bouchez, J., Gaillardet, J., 2014. How accurate are rivers as gauges of chemical denudation of the Earth surface ? Geology 42 (2), 171–174.

Bouchez, J., Gaillardet, J., France-Lanord, C., Maurice, L., Dutra-Maia, P., 2011. Grain size control of river suspended sediment geochemistry : Clues from Amazon River depth profiles. Geochem. Geophys. Geosys. 12 (3), Q03008.

Bouchez, J., Gaillardet, J., Lupker, M., Louvat, P., France-Lanord, C., Maurice, L., Armijos, E., Moquet, J., 2012. Floodplains of large rivers : Weathering reactors or simple silos ? Chemical Geology.

Bouchez, J., Gaillardet, J., von Blanckenburg, F., 2014. Weathering intensity in lowland river basins : From the Andes to the Amazon mouth. Procedia Earth and Planetary Science 10, 280–286.

Bouchez, J., von Blanckenburg, F., Schuessler, J. A., 2013. Modeling novel stable isotope ratios in the weathering zone. American Journal of Science 313 (4), 267–308.

Bourgoin, L., Bonnet, M.-P., Martinez, J.-M., Kosuth, P., Cochonneau, G., Moreira-Turcq, P., Guyot, J.-L., Vauchel, P., Filizola, N., Seyler, P., 2007. Temporal dynamics of water and sediment exchanges between the Curuaí floodplain and the Amazon River, Brazil. Journal of Hydrology 335 (1), 140–156.

Brinkmann, W., 1986. Particulate and dissolved materials in the Rio Negro-Amazon Basin. In : Sediments and water interactions. Springer, pp. 3–12.

Bryant, J., Yogodzinski, G., Hall, M., Lewicki, J., Bailey, D., 2006. Geochemical constraints on the origin of volcanic rocks from the Andean Northern Volcanic Zone, Ecuador. Journal of Petrology 47 (6), 1147–1175.

Burton, K., Vigier, N., 2011. Lithium isotopes as tracers in marine and terrestrial environments. Handbook of Environmental Isotope Geochemistry, 41–59.

Cardinal, D., Gaillardet, J., Hughes, H., Opfergelt, S., André, L., 2010. Contrasting silicon isotope signatures in rivers from the Congo Basin and the specific behaviour of organic-rich waters. Geophysical Research Letters 37 (12), L12403.

Cogez, A., Meynadier, L., Allègre, C., Limmois, D., Herman, F., Gaillardet, J., 2015. Constraints on the role of tectonic and climate on erosion revealed by two time series analysis of marine cores around New Zealand. Earth and Planetary Science Letters 410, 174–185.

Deberdt, S., Viers, J., Dupré, B., 2002. New insights about the rare earth elements (REE) mobility in river waters. Bulletin de la Société Géologique de France 173 (2), 147–160.

Dellinger, M., Gaillardet, J., Bouchez, J., Calmels, D., Galy, V., Hilton, R. G., Louvat, P., France-Lanord, C., 2014. Lithium isotopes in large rivers reveal the cannibalistic nature of modern continental weathering and erosion. Earth and Planetary Science Letters 401, 359–372.

Dixon, J., von Blanckenburg, F., 2012. Soils as pacemakers and limiters of global silicate weathering. Comptes Rendus Geoscience.

Do Nascimento, N., Bueno, G., Fritsch, E., Herbillon, A., Allard, T., Melfi, A., Astolfo, R., Boucher, H., Li, Y., 2004. Podzolization as a deferralitization process : a study of an Acrisol–Podzol sequence derived from Palaeozoic sandstones in the northern upper Amazon Basin. European journal of soil science 55 (3), 523–538.

Dosseto, A., Bourdon, B., Gaillardet, J., Allègre, C., Filizola, N., 2006a. Time scale and conditions of weathering under tropical climate : Study of the Amazon basin with U-series. Geochimica et Cosmochimica Acta 70 (1), 71–89.

Dosseto, A., Bourdon, B., Gaillardet, J., Maurice-Bourgoin, L., Allègre, C., 2006b. Weathering and transport of sediments in the Bolivian Andes : time constraints from uranium-series isotopes. Earth and Planetary Science Letters 248 (3), 759–771.

Dunne, T., Mertes, L. A., Meade, R. H., Richey, J. E., Forsberg, B. R., 1998. Exchanges of sediment between the flood plain and channel of the Amazon River in Brazil. Geological Society of America Bulletin 110 (4), 450–467.

Dupré, B., Dessert, C., Oliva, P., Goddéris, Y., Viers, J., François, L., Millot, R., Gaillardet, J., 2003. Rivers, chemical weathering and Earth's climate. Comptes Rendus Geoscience 335 (16), 1141–1160.

Edmond, J., Palmer, M., Measures, C., Brown, E., Huh, Y., 1996. Fluvial geochemistry of the eastern slope of the northeastern andes and its foredeep in the drainage of the orinoco in colombia and venezuela. Geochimica et cosmochimica acta 60 (16), 2949–2974.

Edmond, J., Palmer, M., Measures, C., Grant, B., Stallard, R., 1995. The fluvial geochemistry and denudation rate of the Guayana Shield in Venezuela, Colombia, and Brazil. Geochimica et cosmochimica acta 59 (16), 3301–3325.

Elbaz-Poulichet, F., Seyler, P., Maurice-Bourgoin, L., Guyot, J., Dupuy, C., 1999. Trace element geochemistry in the upper Amazon drainage basin (Bolivia). Chemical geology 157 (3), 319–334.

Ferrier, K. L., Kirchner, J. W., 2008. Effects of physical erosion on chemical denudation rates : a numerical modeling study of soil-mantled hillslopes. Earth and Planetary Science Letters 272 (3), 591–599.

Filizola, N., Guyot, J. L., 2009. Suspended sediment yields in the Amazon basin : an assessment using the Brazilian national data set. Hydrological processes 23 (22), 3207–3215.

Frings, P. J., De La Rocha, C., Struyf, E., Van Pelt, D., Schoelynck, J., Hudson, M. M., Gondwe, M. J., Wolski, P., Mosimane, K., Gray, W., et al., 2014. Tracing silicon cycling in the Okavango Delta, a sub-tropical flood-pulse wetland using silicon isotopes. Geochimica et Cosmochimica Acta 142, 132–148.

Fritsch, E., Balan, E., Régina Do Nascimento, N., Allard, T., Bardy, M., Bueno, G., Derenne, S., Melfi, A., Calas, G., 2011. Deciphering the weathering processes using environmental mineralogy and geochemistry : Towards an integrated model of laterite and podzol genesis in the Upper Amazon Basin. Comptes Rendus Geoscience 343 (2), 188–198.

Froelich, F., Misra, S., 2014. Was the late paleocene-early eocene hot because earth was flat ? an ocean lithium isotope view of mountain building, continental weathering, carbon dioxide, and Earth's Cenozoic climate. Oceanography 27 (1), 36–49.

Gaillardet, J., Dupre, B., Allegre, C., Négrel, P., 1997. Chemical and physical denudation in the Amazon River Basin. Chemical Geology 142 (3), 141–173.

Gaillardet, J., Dupré, B., Louvat, P., Allegre, C., 1999. Global silicate weathering and CO_2 consumption rates deduced from the chemistry of large rivers. Chemical Geology 159 (1-4), 3–30.

Gaillardet, J., Viers, J., Dupré, B., 2014. Trace elements in river waters. Treatise on geochemistry (second edition) 7, 195–235.

Georg, R., Reynolds, B., West, A., Burton, K., Halliday, A., 2007. Silicon isotope variations accompanying basalt weathering

in Iceland. Earth and Planetary Science Letters 261 (3), 476–490.
Gibbs, R. J., 1967. The geochemistry of the Amazon River system : Part i. the factors that control the salinity and the composition and concentration of the suspended solids. Geological Society of America Bulletin 78 (10), 1203–1232.
Gislason, S. R., Arnorsson, S., Armannsson, H., 1996. Chemical weathering of basalt in Southwest Iceland ; effects of runoff, age of rocks and vegetative/glacial cover. American Journal of Science 296 (8), 837–907.
Gurumurthy, G., Balakrishna, K., Riotte, J., Braun, J.-J., Audry, S., Shankar, H., Manjunatha, B., 2012. Controls on intense silicate weathering in a tropical river, southwestern India. Chemical Geology 300, 61–69.
Guyot, J. L., Fillzola, N., Quintanilla, J., Cortez, J., 1996. Dissolved solids and suspended sediment yields in the rio madeira basin, from the bolivian andes to the amazon. IAHS PUBLICATION, 55–64.
Guyot, J.-L., Jouanneau, J., Soares, L., Boaventura, G., Maillet, N., Lagane, C., 2007. Clay mineral composition of river sediments in the amazon basin. Catena 71 (2), 340–356.
Hathorne, E. C., James, R. H., 2006. Temporal record of lithium in seawater : A tracer for silicate weathering ? Earth and Planetary Science Letters 246 (3), 393–406.
Henchiri, S., Clergue, C., Dellinger, M., Gaillardet, J., Louvat, P., Bouchez, J., 2014. The influence of hydrothermal activity on the Li isotopic signature of rivers draining volcanic areas. Procedia Earth and Planetary Science 10, 223–230.
Holland, H., 1984. The chemical evolution of the atmosphere and oceans. Princeton University Press.
Huang, K.-J., Teng, F.-Z., Wei, G.-J., Ma, J.-L., Bao, Z.-Y., 2012. Adsorption-and desorption-controlled magnesium isotope fractionation during extreme weathering of basalt in Hainan Island, China. Earth and Planetary Science Letters 359, 73–83.
Hughes, H., Sondag, F., Santos, R., André, L., Cardinal, D., 2013. The riverine silicon isotope composition of the amazon basin. Geochimica et Cosmochimica Acta 121, 637–651.
Huh, Y., Chan, L., Edmond, J., 2001. Lithium isotopes as a probe of weathering processes : Orinoco river. Earth and Planetary Science Letters 194 (1-2), 189–199.
Huh, Y., Chan, L., Zhang, L., Edmond, J., 1998. Lithium and its isotopes in major world rivers : implications for weathering and the oceanic budget. Geochimica et Cosmochimica Acta 62 (12), 2039–2051.
Imahashi, M., Takamatsu, N., Kato, N., Matsubaya, O., 1993. A geochemical study on the Hot Springs in Peru, 87–97.
James, R. H., Palmer, M. R., 2000. The lithium isotope composition of international rock standards. Chemical Geology 166 (3), 319–326.
Johnson, C. M., Beard, B. L., Albarède, F., 2004. Overview and general concepts. Reviews in Mineralogy and geochemistry 55 (1), 1–24.
Kisakurek, B., James, R., Harris, N., 2005. Li and δ^7li in Himalayan rivers : Proxies for silicate weathering ? Earth and Planetary Science Letters 237 (3-4), 387–401.
Kloppmann, W., Négrel, P., Casanova, J., Klinge, H., Schelkes, K., Guerrot, C., 2001. Halite dissolution derived brines in the vicinity of a Permian salt dome (N German Basin). Evidence from boron, strontium, oxygen, and hydrogen isotopes. Geochimica et Cosmochimica Acta 65 (22), 4087–4101.
Laraque, A., Bernal, C., Bourrel, L., Darrozes, J., Christophoul, F., Armijos, E., Fraizy, P., Pombosa, R., Guyot, J.-L., 2009. Sediment budget of the Napo river, Amazon basin, Ecuador and Peru. Hydrological processes 23 (25), 3509–3524.
Lemarchand, E., Chabaux, F., Vigier, N., Millot, R., Pierret, M., 2010. Lithium isotope systematics in a forested granitic catchment (Strengbach, Vosges Mountains, France). Geochimica et Cosmochimica Acta 74 (16), 4612–4628.
Li, G., Elderfield, H., 2013. Evolution of carbon cycle over the past 100 million years. Geochimica et Cosmochimica Acta 103, 11–25.
Li, G., West, A. J., 2014. Evolution of cenozoic seawater lithium isotopes : Coupling of global denudation regime and shifting seawater sinks. Earth and Planetary Science Letters 401, 284–293.
Lupker, M., France-Lanord, C., Galy, V., Lave, J., Gaillardet, J., Gajurel, A. P., Guilmette, C., Rahman, M., Singh, S. K., Sinha, R., 2012. Predominant floodplain over mountain weathering of Himalayan sediments (Ganga basin). Geochimica et Cosmochimica Acta 84, 410–432.
Maher, K., Chamberlain, C., 2014. Hydrologic regulation of chemical weathering and the geologic carbon cycle. science 343 (6178), 1502–1504.
Mathieu, D., Bernat, M., Nahon, D., 1995. Short-lived U and Th isotope distribution in a tropical laterite derived from granite (Pitinga river basin, Amazonia, Brazil) : application to assessment of weathering rate. Earth and Planetary Science Letters 136 (3), 703–714.
Meade, R. H., Nordin, C. F., Curtis, W. F., Rodrigues, F. M. C., Do Vale, C. M., Edmond, J. M., 1979. Sediment loads in the Amazon River.
Millot, R., Girard, J., 2007. Lithium isotope fractionation during adsorption onto mineral surfaces. In : International Meeting on Clays in Natural & Engineered Barriers for Radioactive Waste Confinement, Lille, France.

Millot, R., Giraud, E. P., Guerrot, C., Négrel, P., et al., 2010a. Multi-isotopic composition (delta Li-7-delta B-11-delta D-delta O-18) of rainwaters in France : Origin and spatio-temporal characterization. Applied Geochemistry 25 (10).

Millot, R., Guerrot, C., Vigier, N., 2007. Accurate and High-Precision Measurement of Lithium Isotopes in Two reference Materials by MC-ICP-MS. Geostandards and Geoanalytical Research 28 (1), 153–159.

Millot, R., Scaillet, B., Sanjuan, B., 2010b. Lithium isotopes in island arc geothermal systems : Guadeloupe, Martinique (French West Indies) and experimental approach. Geochimica et Cosmochimica Acta 74 (6), 1852–1871.

Millot, R., Vigier, N., Gaillardet, J., 2010c. Behaviour of lithium and its isotopes during weathering in the Mackenzie Basin, Canada. Geochimica et Cosmochimica Acta 74 (14), 3897–3912.

Misra, S., Froelich, P., 2012. Lithium isotope history of cenozoic seawater : Changes in silicate weathering and reverse weathering. Science 335 (6070), 818–823.

Moquet, J., Crave, A., Viers, J., Seyler, P., Armijos, E., Bourrel, L., Chavarri, E., Lagane, C., Laraque, A., Casimiro, W., et al., 2011. Chemical weathering and atmospheric/soil CO_2 uptake in the Andean and Foreland Amazon basins. Chemical Geology 287 (1), 1–26.

Moreira-Turcq, P., Seyler, P., Guyot, J. L., Etcheber, H., 2003. Exportation of organic carbon from the Amazon River and its main tributaries. Hydrological Processes 17 (7), 1329–1344.

Mortatti, J., Probst, J.-L., 2003. Silicate rock weathering and atmospheric/soil CO_2 uptake in the Amazon basin estimated from river water geochemistry : seasonal and spatial variations. Chemical Geology 197 (1), 177–196.

Nesbitt, H., Young, G., 1982. Early proterozoic climates and plate motions inferred from major element chemistry of lutites. Nature 299 (5885), 715–717.

Palmer, M., Edmond, J., 1992. Controls over the strontium isotope composition of river water. Geochimica et Cosmochimica Acta 56 (5), 2099–2111.

Petford, N., Atherton, M., 1996. Na-rich partial melts from newly underplated basaltic crust : the Cordillera Blanca Batholith, Peru. Journal of Petrology 37 (6), 1491–1521.

Pistiner, J., Henderson, G., 2003. Lithium-isotope fractionation during continental weathering processes. Earth and Planetary Science Letters 214 (1), 327–339.

Pogge von Strandmann, P., Burton, K., James, R., van Calsteren, P., Gislason, S., Mokadem, F., 2006. Riverine behaviour of uranium and lithium isotopes in an actively glaciated basaltic terrain. Earth and Planetary Science Letters 251 (1-2), 134–147.

Pogge von Strandmann, P., Burton, K., James, R., Van Calsteren, P., Gislason, S., et al., 2010. Assessing the role of climate on uranium and lithium isotope behaviour in rivers draining a basaltic terrain. Chemical Geology 270 (1-4), 227–239.

Pogge von Strandmann, P. A., Burton, K. W., James, R. H., Van Calsteren, P., Gislason, S. R., Sigfússon, B., 2008. The influence of weathering processes on riverine magnesium isotopes in a basaltic terrain. Earth and Planetary Science Letters 276 (1), 187–197.

Pogge von Strandmann, P. A., Henderson, G. M., 2015. The Li isotope response to mountain uplift. Geology 43 (1), 67–70.

Pogge von Strandmann, P. A., Jenkyns, H. C., Woodfine, R. G., 2013. Lithium isotope evidence for enhanced weathering during Oceanic Anoxic Event 2. Nature Geoscience 6 (8), 668–672.

Pogge von Strandmann, P. A., Opfergelt, S., Lai, Y.-J., Sigfússon, B., Gislason, S. R., Burton, K. W., 2012. Lithium, magnesium and silicon isotope behaviour accompanying weathering in a basaltic soil and pore water profile in Iceland. Earth and Planetary Science Letters 339, 11–23.

Pogge von Strandmann, P. A., Porcelli, D., James, R. H., van Calsteren, P., Schaefer, B., Cartwright, I., Reynolds, B. C., Burton, K. W., 2014. Chemical weathering processes in the Great Artesian Basin : Evidence from lithium and silicon isotopes. Earth and Planetary Science Letters 406, 24–36.

Raymo, M., Ruddiman, W., 1992. Tectonic forcing of late Cenozoic climate. Nature 359 (6391), 117–122.

Reeder, S., Hitchon, B., Levinson, A., 1972. Hydrogeochemistry of the surface waters of the Mackenzie River drainage basin, Canada I. Factors controlling inorganic composition. Geochimica et Cosmochimica Acta 36 (8), 825–865.

Riebe, C. S., Kirchner, J. W., Granger, D. E., Finkel, R. C., 2001. Strong tectonic and weak climatic control of long-term chemical weathering rates. Geology 29 (6), 511–514.

Roddaz, M., Viers, J., Brusset, S., Baby, P., Hérail, G., 2005. Sediment provenances and drainage evolution of the Neogene Amazonian foreland basin. Earth and Planetary Science Letters 239 (1), 57–78.

Ronov, A., Migdisov, A., Voskresenskaya, N., Korzina, G., 1970. Geochemistry of lithium in the sedimentary cycle.

Ryu, J.-S., Vigier, N., Lee, S.-W., Lee, K.-S., Chadwick, O. A., 2014. Variation of lithium isotope geochemistry during basalt weathering and secondary mineral transformations in hawaii. Geochimica et Cosmochimica Acta 145, 103–115.

Safran, E. B., Bierman, P. R., Aalto, R., Dunne, T., Whipple, K. X., Caffee, M., 2005. Erosion rates driven by channel network incision in the Bolivian Andes. Earth Surface Processes and Landforms 30 (8), 1007–1024.

961 Santos, R. V., Sondag, F., Cochonneau, G., Lagane, C., Brunet, P., Hattingh, K., Chaves, J. G., 2014. Source area and seasonal
962 $^{87}sr/^{86}sr$ variations in rivers of the Amazon basin. Hydrological Processes.
963 Sarbas, B., Nohl, U., 2008. The georoc database as part of a growing geoinformatics network. Geoinformatics.
964 Sawhney, B., 1972. Selective sorption and fixation of cations by clay minerals : a review. Clays Clay Miner 20, 93–100.
965 Stallard, R., Edmond, J., 1981. Geochemistry of the Amazon 1. Precipitation chemistry and the marine contribution to the
966 dissolved load at the time of peak discharge. Journal of Geophysical Research 86 (C10), 9844–9858.
967 Stallard, R., Edmond, J., 1983. Geochemistry of the Amazon 2. the influence of geology and weathering environment on the
968 dissolved load. Journal of Geophysical Research 88 (C14), 9671–9688.
969 Stallard, R., Edmond, J., 1987. Geochemistry of the Amazon 3. Weathering chemistry and limits to dissolved inputs. Journal
970 of geophysical Research 92 (C8), 8293–8302.
971 Taylor, S. R., McLennan, S. M., 1985. The continental crust : its composition and evolution.
972 Teng, F.-Z., Rudnick, R. L., McDonough, W. F., Gao, S., Tomascak, P. B., Liu, Y., 2008. Lithium isotopic composition and
973 concentration of the deep continental crust. Chemical Geology 255 (1), 47–59.
974 Tipper, E., Calmels, D., Gaillardet, J., Louvat, P., Capmas, F., Dubacq, B., 2012. Positive correlation between Li and Mg
975 isotope ratios in the river waters of the Mackenzie Basin challenges the interpretation of apparent isotopic fractionation
976 during weathering. Earth and Planetary Science Letters 333, 35–45.
977 Tipper, E., Galy, A., Bickle, M., 2006. Riverine evidence for a fractionated reservoir of ca and mg on the continents : implications
978 for the oceanic ca cycle. Earth and Planetary Science Letters 247 (3), 267–279.
979 Torres, M. A., West, A. J., Li, G., 2014. Sulphide oxidation and carbonate dissolution as a source of CO_2 over geological
980 timescales. Nature 507 (7492), 346–349.
981 Verney-Carron, A., Vigier, N., Millot, R., 2011. Experimental determination of the role of diffusion on Li isotope fractionation
982 during basaltic glass weathering. Geochimica et Cosmochimica Acta 75 (12), 3452–3468.
983 Viers, J., Dupré, B., Braun, J.-J., Deberdt, S., Angeletti, B., Ngoupayou, J. N., Michard, A., 2000. Major and trace element
984 abundances, and strontium isotopes in the Nyong basin rivers (Cameroon) : constraints on chemical weathering processes
985 and elements transport mechanisms in humid tropical environments. Chemical Geology 169 (1), 211–241.
986 Viers, J., Dupré, B., Polvé, M., Schott, J., Dandurand, J., Braun, J., 1997. Chemical weathering in the drainage basin of
987 a tropical watershed (nsimi-zoetele site, cameroon) : comparison between organic-poor and organic-rich waters. Chemical
988 Geology 140 (3), 181–206.
989 Vigier, N., Decarreau, A., Millot, R., Carignan, J., Petit, S., France-Lanord, C., 2008. Quantifying Li isotope fractionation
990 during smectite formation and implications for the Li cycle. Geochimica et Cosmochimica Acta 72 (3), 780–792.
991 Vigier, N., Decarreau, A., Petit, S., Turpault, M., 2011. Li isotope compositions of clay minerals : what message ? In : AGU
992 Fall Meeting Abstracts. Vol. 1. p. 02.
993 Vigier, N., Gislason, S., Burton, K., Millot, R., Mokadem, F., 2009. The relationship between riverine lithium isotope compo-
994 sition and silicate weathering rates in Iceland. Earth and Planetary Science Letters 287 (3), 434–441.
995 Walker, J., Hays, P., Kasting, J., 1981. A negative feedback mechanism for the long-term stabilization of the Earth's surface
996 temperature. Journal of Geophysical Research 86 (C10), 9776–9782.
997 Wang, Q.-L., Chetelat, B., Zhao, Z.-Q., Ding, H., Li, S.-L., Wang, B.-L., Li, J., Liu, X.-L., 2015. Behavior of lithium isotopes
998 in the changjiang river system : Sources effects and response to weathering and erosion. Geochimica et Cosmochimica Acta
999 151, 117–132.
1000 Wanner, C., Sonnenthal, E. L., Liu, X.-M., 2014. Seawater δ^7li : A direct proxy for global CO2 consumption by continental
1001 silicate weathering ? Chemical Geology 381, 154–167.
1002 West, A., Galy, A., Bickle, M., 2005. Tectonic and climatic controls on silicate weathering. Earth and Planetary Science Letters
1003 235 (1-2), 211–228.
1004 West, A. J., 2012. Thickness of the chemical weathering zone and implications for erosional and climatic drivers of weathering
1005 and for carbon-cycle feedbacks. Geology 40 (9), 811–814.
1006 West, A. J., Bickle, M. J., Collins, R., Brasington, J., 2002. Small-catchment perspective on himalayan weathering fluxes.
1007 Geology 30 (4), 355–358.
1008 Willenbring, J. K., Von Blanckenburg, F., 2010. Long-term stability of global erosion rates and weathering during late-cenozoic
1009 cooling. Nature 465 (7295), 211–214.
1010 Wimpenny, J., Colla, C. A., Yin, Q.-Z., Rustad, J. R., Casey, W. H., 2014. Investigating the behaviour of mg isotopes during
1011 the formation of clay minerals. Geochimica et Cosmochimica Acta 128, 178–194.
1012 Wimpenny, J., Gíslason, S. R., James, R. H., Gannoun, A., Pogge Von Strandmann, P. A., Burton, K. W., 2010a. The
1013 behaviour of Li and Mg isotopes during primary phase dissolution and secondary mineral formation in basalt. Geochimica
1014 et Cosmochimica Acta 74 (18), 5259–5279.

Wimpenny, J., James, R. H., Burton, K. W., Gannoun, A., Mokadem, F., Gíslason, S. R., 2010b. Glacial effects on weathering processes : New insights from the elemental and lithium isotopic composition of West Greenland rivers. Earth and Planetary Science Letters 290 (3), 427–437.

Wittmann, H., Von Blanckenburg, F., Guyot, J.-L., Maurice, L., Kubik, P., 2009. From source to sink : Preserving the cosmogenic ^{10}be-derived denudation rate signal of the Bolivian Andes in sediment of the Beni and Mamoré foreland basins. Earth and Planetary Science Letters 288 (3), 463–474.

Wittmann, H., von Blanckenburg, F., Maurice, L., Guyot, J.-L., Filizola, N., Kubik, P. W., 2011. Sediment production and delivery in the Amazon river basin quantified by in situ–produced cosmogenic nuclides and recent river loads. Geological Society of America Bulletin 123 (5-6), 934–950.

Zhang, L., Chan, L.-H., Gieskes, J. M., 1998. Lithium isotope geochemistry of pore waters from ocean drilling program sites 918 and 919, irminger basin. Geochimica et Cosmochimica Acta 62 (14), 2437–2450.

1026 **Figures**

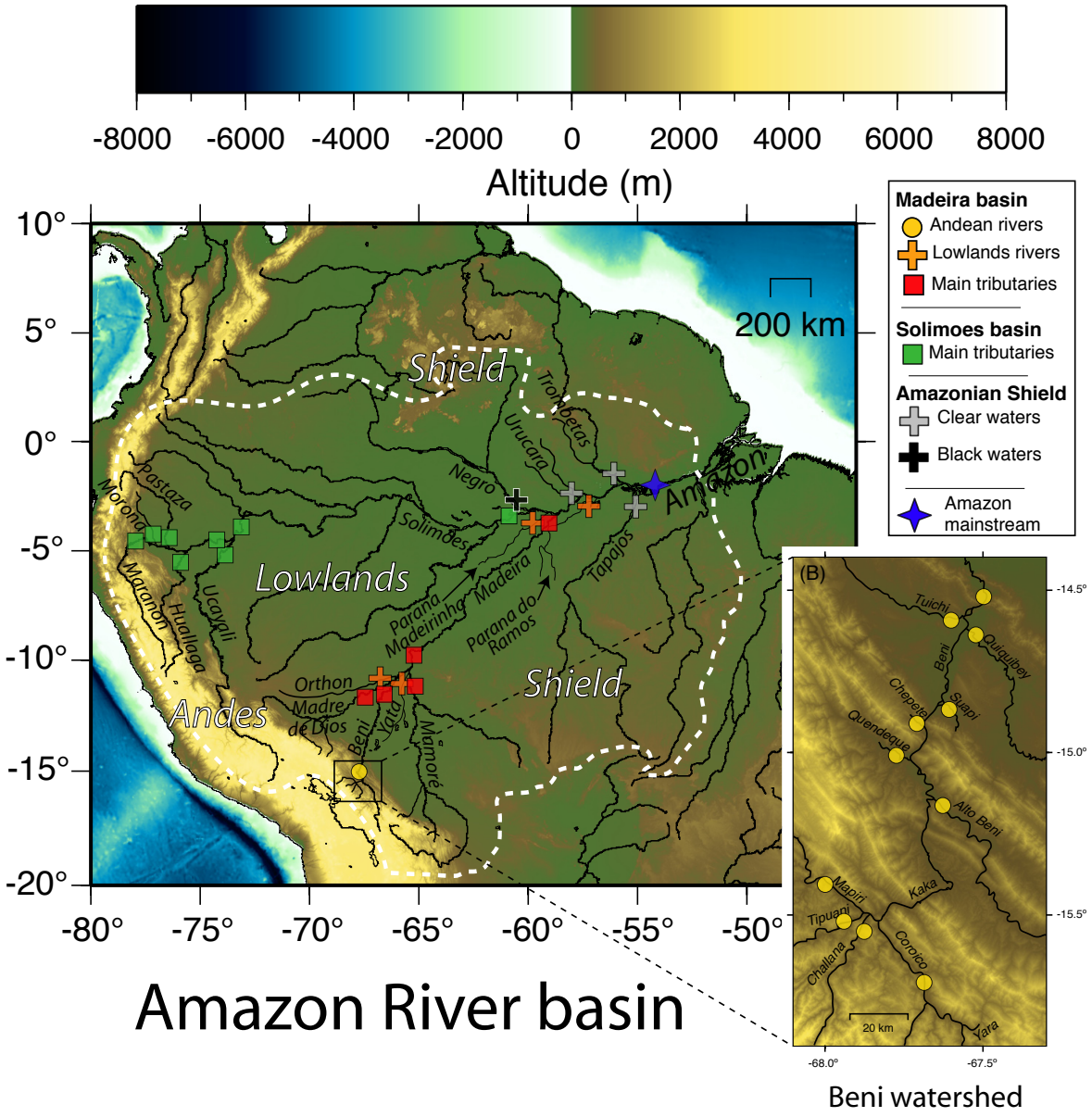

FIGURE 1: Map of the Amazon River basin with the location of river samples.

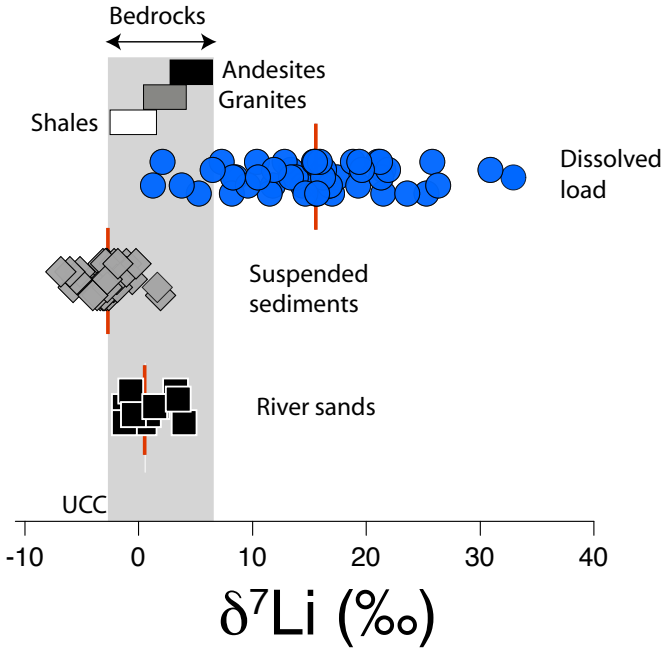

FIGURE 2: Li isotope composition in Amazon river-borne material. The red marker indicates the mean isotope composition in each component. Suspended sediment and sands data are from Dellinger et al. (2014). Reported bedrock data are global mean δ^7Li of shales (-0.5±1.9‰), andesites (+4.8±1.4‰) and granodiorites (+2.0±2.2‰) from the literature compiled in Dellinger et al. (2014).

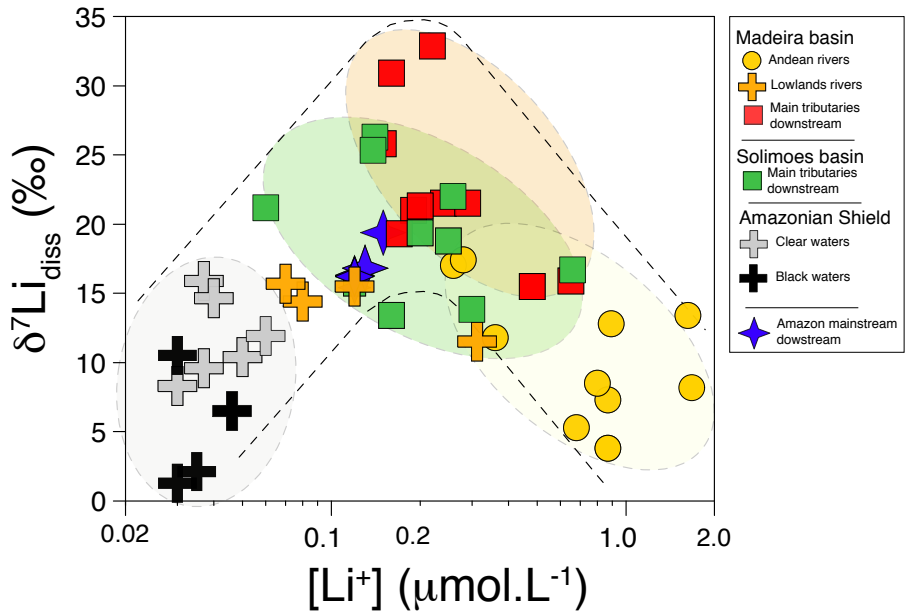

FIGURE 3: Li isotope composition (δ^7Li_{diss}) as a function of the Li concentration in the dissolved load. Data from Huh et al. (1998) of Amazon tributaries (Negro, Solimões, Madeira and Amazon) are also displayed on this figure and the following figures of this publication.

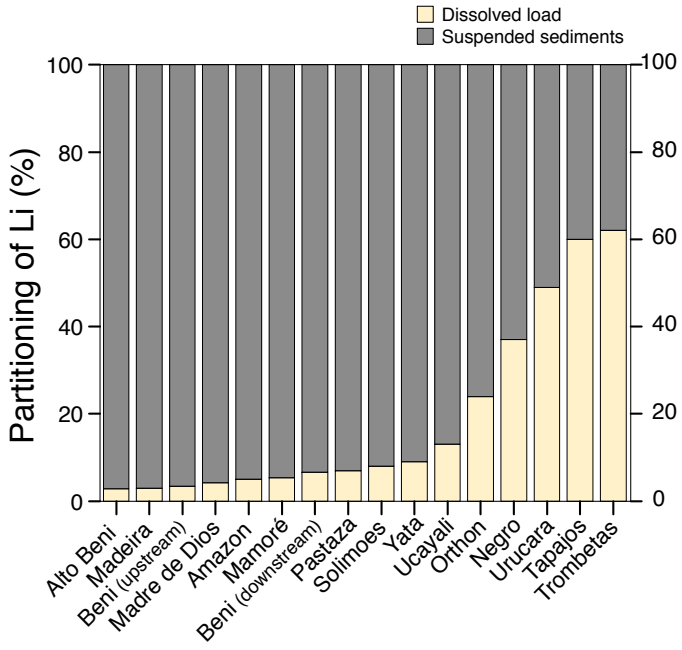

FIGURE 4: Partitioning of Li between the dissolved and particulate load. Only Li concentration measured in surface suspended sediments was used in Eq. (1).

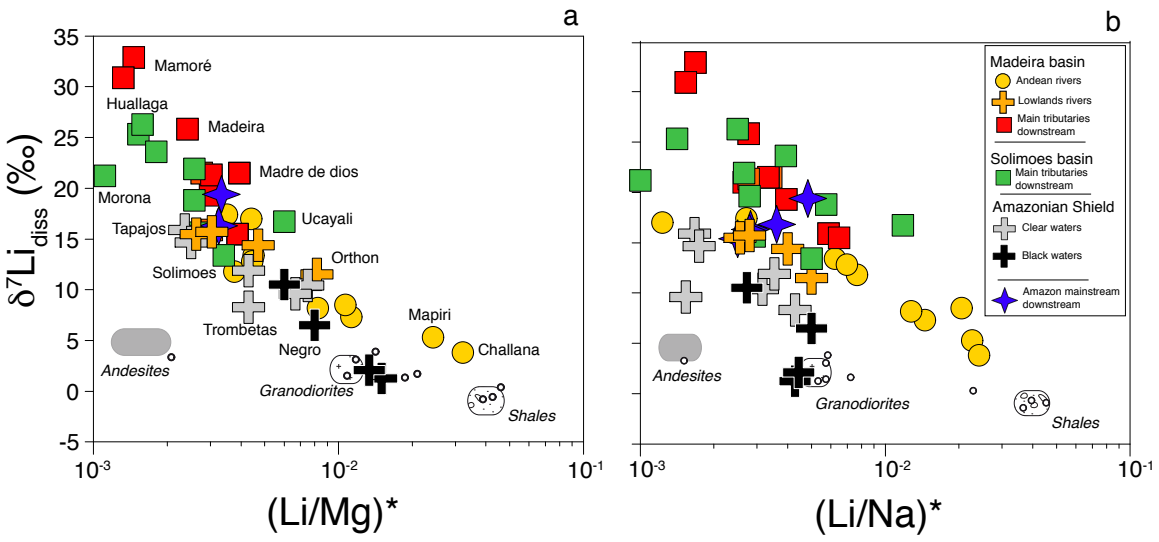

FIGURE 5: Dissolved Li isotope composition (δ^7Li) vs a) (Li/Mg)* and b) (Li/Na)* molar ratios. The superscript "*" indicates that molar ratios are corrected for rainwater and evaporite inputs. Typical bedrock ratios and Amazon river sands are added for comparison.

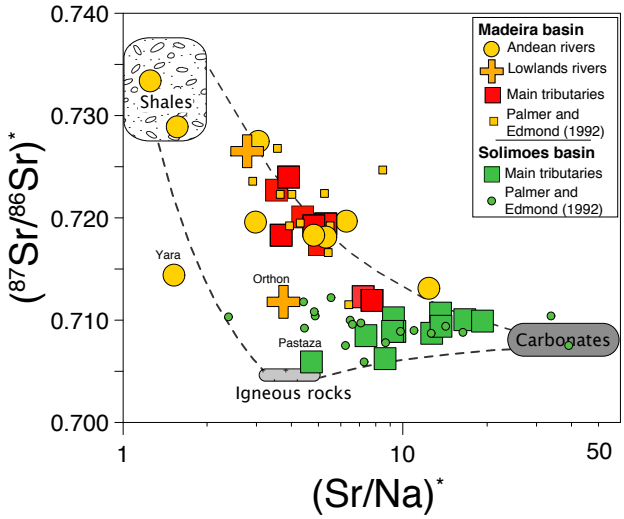

FIGURE 6: Dissolved (^{87}Sr/^{86}Sr)* versus (Sr/Na)* in the Amazon River system. The superscript "*" means that the data are corrected for rainwater and evaporite inputs. "Igneous rocks" refers to Andean andesites and granodiorites in the Amazon Basin

. Data from Palmer and Edmond (1992) are also represented while rivers draining only the Brazilian and Guiana shield are not displayed. The endmembers (shale, igneous rocks and carbonates) correspond to the chemical composition of water masses draining each type of rock and defined in Appendix A.

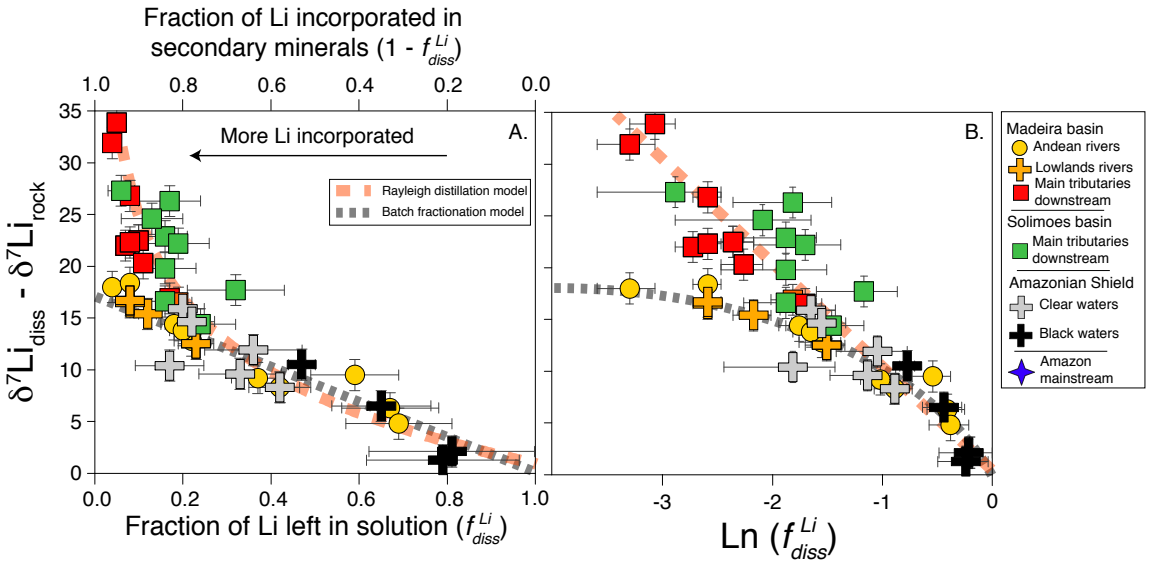

FIGURE 7: Li isotope composition of the dissolved load corrected from the composition of the bedrock (δ^7Li_{diss} - δ^7Li_{rock}) vs. a) the fraction of Li remaining in solution (f^{Li}_{diss}) and b) the natural logarithm of (1 - f^{Li}_{diss}). The fitted expected Rayleigh distillation and "batch" trends are represented in red and black dotted lines respectively. The δ^7Li_{rock} corresponds to the δ^7Li_0 calculated for each river using the mixing proportion of Li given in the Table (7) and the mean Li isotope composition of each bedrock. For rivers draining only shales, the right Y-intercept of the line in the δ^7Li_{diss}-f^{Li}_{diss} space gives an accurate estimate of the source shale bedrock of -1.0±0.3‰.

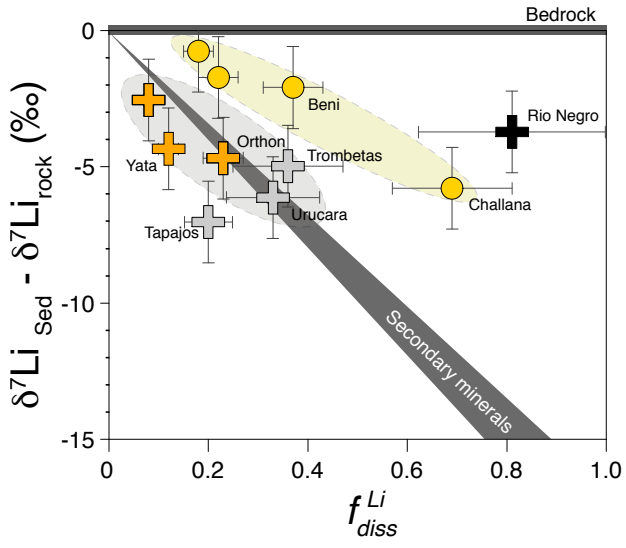

FIGURE 8: The (δ^7Li_{sed} - δ^7Li_{rock}) as a function of the fraction of Li remaining in solution (f^{Li}_{diss}). Here "sed" refers only to surface suspended sediments. The grey envelope corresponds to the theoretical Li isotope composition predicted by a "batch" fractionation model with a fractionation factor of 0.983 ± 0.002. The black line corresponds to the isotope composition of the bedrock.

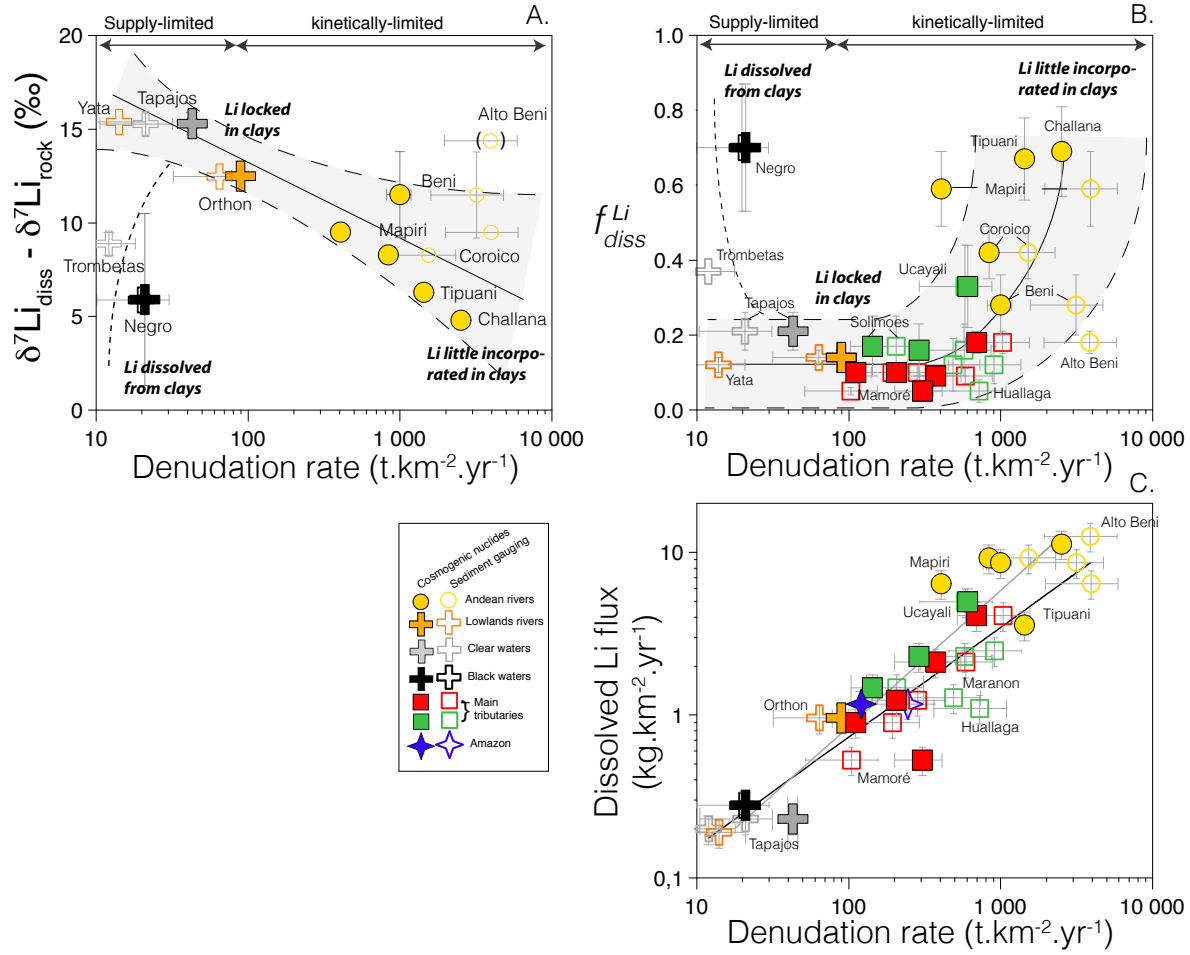

FIGURE 9: a) Li isotope composition of the dissolved load corrected from the composition of the bedrock (δ^7Li_{diss} - δ^7Li_{rock}) as a function of denudation rates for rivers fitting the "batch" fractionation model. The other rivers are not represented on this diagram. Both cosmogenic nuclide-derived (closed symbols) and sediment gauging-derived (open symbols) denudation rates are represented. The black line represents the correlation between δ^7Li_{diss} - δ^7Li_{rock} and the denudation rate and is similar to the trend modelled by Bouchez et al. (2013). The Alto Beni river does not plot on the correlation defined by other rivers, its present-day denudation flux might be too high because of recent mobilization of plio-quaternary sediments (Dosseto et al., 2006b). (b) fraction of Li left in solution (f^{Li}_{diss}) as the function of the denudation rate. f^{Li}_{diss} values are less than 0.2 for denudation rates inferior to 1000 $t.km^{-2}.yr^{-1}$ and increase for higher denudation rates (c) Specific dissolved flux of lithium as a function of the denudation rate. The black line represents the best fit for the sediment-gauging derived denudation rate (r^2 = 0.91), the grey line represents the best fit for the cosmogenic derived denudation rate (r^2 = 0.78)

.

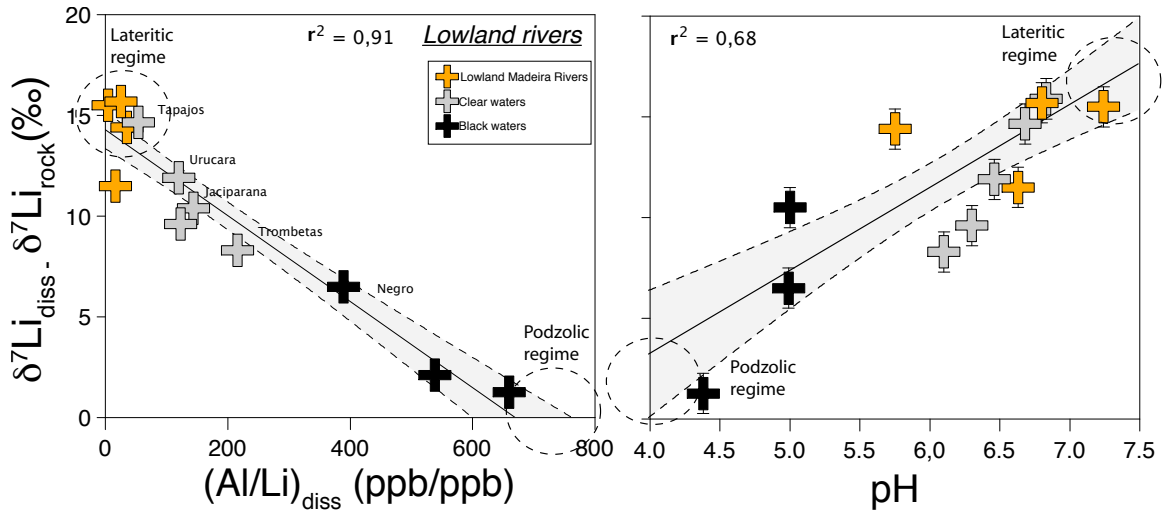

FIGURE 10: Dissolved Li isotope composition corrected from the composition of the bedrock (δ^7Li_{diss} - δ^7Li_{rock}) of the lowland rivers vs. the dissolved Al/Li ratio and pH. River samples can be interpreted as mixture of two types of waters derived from podzolic and lateritic regimes of weathering.

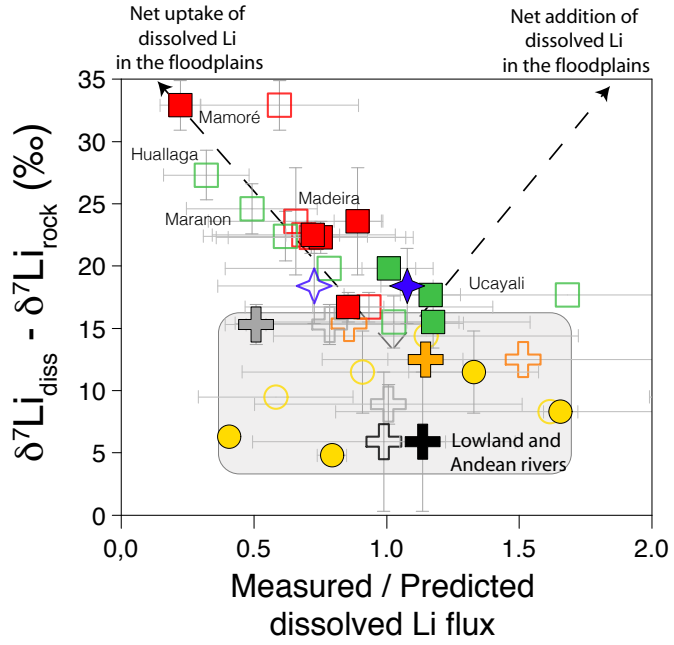

FIGURE 11: Dissolved Li isotope composition corrected from the composition of the bedrock δ^7Li_{diss} - δ^7Li_{rock} vs. the ratio between the predicted and measured dissolved Li flux. The predicted dissolved Li flux is calculated using the equation of the correlation of Fig. (9c) for both cosmogenic nuclides and sediment gauging-derived denudation rates.

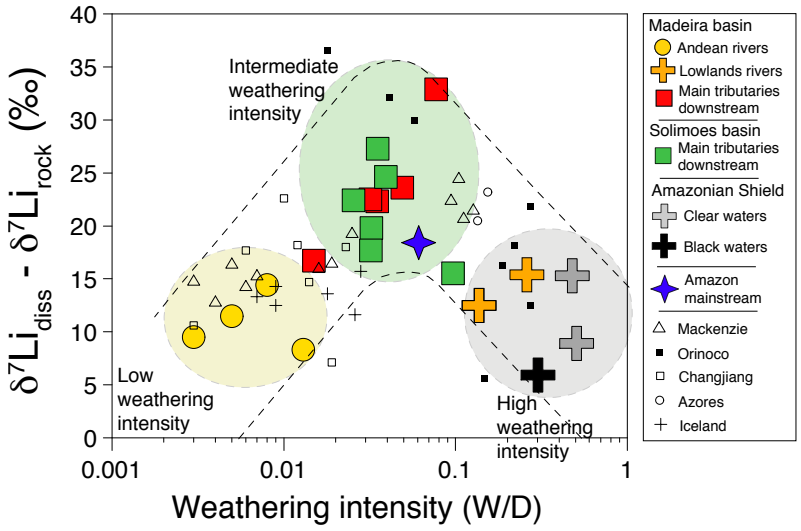

FIGURE 12: Dissolved Li isotope composition corrected from the composition of the bedrock δ^7Li_{diss} - δ^7Li_{rock} vs. silicate weathering intensity, calculated as the ratio between silicate chemical weathering rates and total denudation rate (inferred from decadal sediment gauging measurements). Lithium isotope data for other river systems are from Huh et al. (2001); Pogge von Strandmann et al. (2006, 2010); Vigier et al. (2009); Millot et al. (2010c); Wang et al. (2015) Rivers influenced by hydrothermal weathering are not plotted on this figure because their Li isotope composition is controlled by the input from hot springs (Henchiri et al., 2014) rather than the weathering intensity. References for the compiled or calculated weathering intensity data are given in supplementary materials (table S3).

List of captions

Table 1 : Dissolved major and trace element concentrations and Li-Sr isotope composition of rivers. All concentrations are in in μmol.L^{-1} except Al concentrations (in ppb)

Table 2 : Li concentration and isotope composition of Amazon tributaries surface sediments

Table 3 : Proportion of lithium initially dissolved from each source, and fraction of silicate-derived Li incorporated in secondary minerals

Table 1

Sample	Rivers	Location	pH	Surface SPM (mg/L)	δ^7Li (‰)	Li	Na	K	Mg	Ca	HCO_3	Cl	NO_3	SO_4	NICB	SiO_2	$^{87}Sr/^{86}Sr$	Sr	Al (ppb)
	Madeira Basin																		
AM01-01	Huarinilla	-	-	-	11.8	0.36	51	8	97	41	207	4	15	49	2.6	117	0.72740	0.14	17
AM01-02	Yara	-	-	-	-	0.56	44	3	34	17	-	1	16	44	-	-	0.71442	0.07	15
AM01-03	Yara	-	-	-	-	0.82	90	16	120	90	197	7	24	143	2.5	149	-	0.24	22
AM01-04	Coroico	Guanay	6.5	387	7.3	0.87	62	12	78	55	116	2	14	95	5.1	136	-	0.14	14
AM01-05	Tipuani	Guanay	5.7	1518	5.3	0.68	31	16	28	14	9	2	5	57	0.1	101	-	0.05	4
AM01-06	Challana	Guanay	6.4	1610	3.8	0.87	37	12	28	12	16	1	15	48	1.5	114	0.73331	0.05	15
AM01-07	Mapiri	Guanay	7.2	1620	8.5	0.80	44	16	75	119	-	6	-	6	-	107	0.71969	0.25	10
AM01-08	Alto Beni	Mouth	7.8	8399	13.4	1.62	282	57	359	416	875	25	7	443	5.1	124	0.71921	0.80	20
AM01-09	Quendeque	Mouth	7.4	-	-	0.10	34	24	59	228	484	2	12	67	0.2	89	0.71311	0.41	32
AM01-10	Chepete	Mouth	7.2	1111	17.0	0.26	222	32	60	105	461	12	5	53	0.0	-	0.72847	0.34	8
AM01-11	Suapi	Mouth	7.2	141	-	0.15	39	36	45	202	415	3	12	52	6.3	128	-	-	14
AM01-12	Quiquibey	Mouth	7.5	1895	17.4	0.28	106	43	80	324	821	3	10	54	1.6	-	-	-	11
AM01-13	Tuichi	Mouth	6.4	3590	-	0.53	44	25	54	106	100	2	3	142	0.1	87	0.72103	-	8
AM01-14	Beni	Rurrenabaque	7.4	5265	12.8	0.89	138	38	199	328	575	13	12	310	0.8	-	0.71816	0.61	21
AM07-04	Beni	Rurrenabaque	6.4	109	8.2	1.67	164	25	204	286	520	34	7	283	3.2	159	0.71759	0.74	
AM01-16	Beni	Riberalta	7.0	1036	15.9	0.65	119	48	212	290	640	11	14	231	3.6	137	0.71932	0.58	28
AM07-09	Beni	Riberalta	6.7	1003	15.5	0.48	87	33	125	197	442	15	9	104	11.2	129	0.71911	0.40	-
AM01-15	Madre de Dios	Riberalta	6.9	950	21.5	0.24	72	30	61	171	435	3	11	57	0.6	139	0.71233	0.51	3
AM07-14	Madre de Dios	Riberalta	5.9	437	21.0	0.19	77	28	63	190	451	6	10	43	9.3	130	0.71191	0.56	-
AM01-17	Orthon	Mouth	6.6	460	11.5	0.31	66	41	39	62	256	4	4	3	12.9	-	0.71180	0.23	36
AM01-18	Yata	Mouth	5.8	56	14.4	0.08	22	15	18	12	63	2	4	1	24.6	91	0.72643	0.06	20
AM01-19	Mamoré	Guayaramerin	6.7	507	32.9	0.22	155	48	146	202	497	32	11	162	3.8	153	0.72157	0.48	8
AM07-19	Mamoré	Guayaramerin	6.5	156	30.9	0.16	137	71	122	162	484	35	7	77	11.9	197	0.72258	0.45	-
AM6/1-6	Parana Madeirinha	Mouth	7.2	-	15.5	0.12	108	23	45	205	510	68	-	25	0.2	-	-	-	4
AM6/1-11	Parana do Ramos	Mouth	6.8	-	15.7	0.07	40	15	25	61	179	18	1	15	0.5	-	-	-	13
AM01-20	Jaciparana	Mouth	-	-	10.4	0.06	23	28	8	12	76	4	7	2	1.5	112	0.75620	0.04	60
AM01-21	Madeira	Porto Velho	-	-	21.5	0.29	99	38	106	173	438	14	12	123	-2.2	139	0.71718	0.45	7
AM06-35	Madeira	Foz Madeira	6.9	219	19.3	0.17	58	32	58	101	274	17	12	49	1.8	125	-	0.30	5
AM05-16	Madeira	Foz Madeira	-	85	21.3	0.20	90	29	68	115	275	21	8	60	12.4	151	0.71816	0.27	3
	Solimoes Basin																		
AM08-33	Maranon	Borja	8.1	845	21.9	0.26	185	25	100	455	773	92	11	120	15.4	176	-	-	-
AM08-34	Morona	Mouth	-	174	21.2	0.06	84	21	56	182	381	21	13	20	21.6	226	0.70629	0.58	-

Sample	Rivers	Location	pH	Surface SPM	δ^7Li	Li	Na	K	Mg	Ca	HCO_3	Cl	NO_3	SO_4	NICB	SiO_2	$^{87}Sr/^{86}Sr$	Sr	Al
AM08-36	Pastaza	Mouth	-	102	25.3	0.14	168	28	94	117	364	70	9	31	18.3	293	0.70629	0.56	-
AM08-38	Huallaga	Mouth	-	335	26.3	0.14	1660	32	96	653	986	1621	7	187	6.4	180	0.70904	1.52	-
AM08-40	Tigre	Nueva York	-	25	13.8	0.30	498	16	33	81	90	666	8	9	-5.3	159	0.71671	1.14	-
AM08-05	Amazonas	Tamshiyacu	7.4	344	18.8	0.25	397	36	97	607	1010	358	8	98	14.7	176	0.70917	1.20	-
AM08-24	Maranon	San Regis	7.4	177	23.6	0.12	477	29	82	502	803	445	-	76	16.3	182	0.70878	0.97	-
AM08-13	Ucayali	Jenaro Herrera	-	490	16.7	0.66	308	40	114	683	1109	254	16	128	15.8	153	0.70943	1.43	-
AM05-4	Solimoes	Manacapuru	6.8	283	15.6	0.12	125	25	48	213	-	86	13	27	-	180	-	-	-
AM06-15	Solimoes	Manacapuru	-	333	13.4	0.16	101	20	50	188	443	71	12	34	0.4	158	0.70918	0.53	-
Amazon river mainstream																			
AM05-13	Amazonas	Iracema	-	47	16.3	0.12	85	21	37	136	240	49	10	22	23.6	141	-	0.38	-
AM06-63	Amazonas	Obidos	6.8	127	15.4	0.12	105	21	39	165	355	64	10	22	11.6	146	-	0.44	-
AM05-37	Amazonas	Obidos	-	175	16.8	0.13	81	20	36	131	242	49	1	20	23.2	140	-	0.32	-
AM05-35	Amazonas	Obidos	-	318	16.2	0.12	86	21	38	138	241	49	4	21	26.2	144	-	0.33	-
AM05-39	Amazonas	Obidos	-	250	19.4	0.15	85	23	48	158	352	56	9	35	5.9	135	-	0.32	-
Shield rivers																			
AM6/1-20	Tapajós	Mouth	6.8	-	15.9	0.037	33	22	17.9	23.5	114	10.5	9.7	1.6	0.3	-	-	-	-
Tapajos 19	Tapajós	Mouth	6.7	6	14.7	0.039	33	21	17.0	21.0	114	12.0	-	3.0	-1.5	160	0.73317	0.10	15
AM6/1-13	Trombetas	Mouth	6.3	-	9.6	0.037	39	17	7.7	11.1	71	14.9	3.3	2.2	0.6	-	-	-	34
Trombetas 16	Trombetas	Mouth	6.1	13	8.3	0.037	31	23	9.0	11.0	39	21.0	-	4.0	27.7	103	0.73230	0.08	45
Urucara 10	Urucara	Mouth	6.5	8	11.9	0.049	35	36	16.0	35.0	140	21.0	-	6.0	0.0	105	0.72358	0.15	50
AM6/1-2	Rio Negro	Paricatuba	4.4	-	1.3	0.027	12	6	2.5	4.1	13	5.7	8.8	1.6	0.6	-	-	-	137
AM06-20	Rio Negro	Paricatuba	5.0	4	6.5	0.037	19	7	6.1	-	21	12.7	6.8	3.7	-	84	-	0.08	108
AM01-22	Rio Negro	Paricatuba	-	-	2.1	0.035	14	5	3.1	4.5	20	6.1	6.2	1.0	1.1	-	-	0.03	149

Table 2

Sample	Rivers	Li	δ^7Li MES
Lowland and shield rivers		ppm	
AM6/1-11	Parana dos Ramos	27	-3.6
AM01-17	Orthon	59	-5.7
AM01-18	Yata	100	-5.3
AM01-27	Trombetas	20	-5.1
AM01-22 MES Negro	Negro	44	-2.7
AM6/1-09 MES	Urucara	43	-4.0
AM6/1-20 Tapajos	Tapajos	24	-5.4
AM01-29	Tapajos	27	-6.0
Madeira basin			
AM01-01	Huarinilla	89	-2.7
AM01-06	Challana	91	-6.8
AM01-08	Alto Beni	79	-1.8

Table 3

Samples	Rivers	Location	fLi	Proportion of Li dissolved from each source (%)					δ^7Li_0
				rain	eva	car	sha	ign	
Madeira Basin									
AM01-01	Huarinilla	-	0.22 ± 0.04	0.1	0.0	0.2	99.8	0.0	-1.0
AM01-02	Yara	-	0.38 ± 0.06	0.0	0.0	0.0	99.9	0.0	-1.0
AM01-03	Yara	-	0.28 ± 0.05	0.0	0.0	0.2	99.8	0.0	-1.0
AM01-04	Coroico	Guanay	0.42 ± 0.07	0.0	0.0	0.1	99.9	0.0	-1.0
AM01-05	Tipuani	Guanay	0.67 ± 0.11	0.0	0.0	0.0	100.0	0.0	-1.0
AM01-06	Challana	Guanay	0.69 ± 0.12	0.0	0.0	0.0	100.0	0.0	-1.0
AM01-07	Mapiri	Guanay	0.59 ± 0.10	0.0	0.0	0.2	99.7	0.0	-0.9
AM01-08	Alto Beni	Mouth	0.18 ± 0.03	0.0	0.0	0.4	99.6	0.0	-0.9
AM01-09	Quendeque	Mouth	0.09 ± 0.01	0.1	0.0	3.4	96.5	0.0	-0.1
AM01-10	Chepete	Mouth	0.04 ± 0.01	0.2	0.0	0.6	99.2	0.0	-0.8
AM01-11	Suapi	Mouth	0.12 ± 0.02	0.1	0.0	2.0	97.9	0.0	-0.5
AM01-12	Quiquibey	Mouth	0.08 ± 0.01	0.1	0.0	1.7	98.2	0.0	-0.5
AM01-13	Tuichi	Mouth	0.36 ± 0.06	0.0	0.0	0.3	99.7	0.0	-0.9
AM01-14	Beni	Rurrenabaque	0.20 ± 0.03	0.0	0.0	0.6	99.4	0.0	-0.9
AM07-04	Beni	Rurrenabaque	0.37 ± 0.06	0.0	0.0	0.3	99.7	0.0	-0.9
AM01-16	Beni	Riberalta	0.17 ± 0.03	0.1	0.0	0.7	99.3	0.0	-0.8
AM07-09	Beni	Riberalta	0.19 ± 0.03	0.1	0.0	0.6	99.3	0.0	-0.8
AM01-15	Madre de Dios	Riberalta	0.10 ± 0.02	0.1	0.0	1.0	98.9	0.0	-0.7
AM07-14	Madre de Dios	Riberalta	0.07 ± 0.01	0.1	0.0	1.5	98.4	0.0	-0.6
AM01-17	Orthon	Mouth	0.23 ± 0.04	0.0	0.0	0.0	93.3	6.7	-0.6
AM01-18	Yata	Mouth	0.12 ± 0.02	0.1	0.0	0.2	99.7	0.0	-0.9
AM01-19	Mamoré	Guayaramerin	0.05 ± 0.01	0.0	0.0	0.1	99.9	0.1	-1.0
AM07-19	Mamoré	Guayaramerin	0.04 ± 0.01	0.0	0.0	0.1	99.9	0.1	-1.0
AM6/1-6	Parana Madeirinha	Mouth	0.08 ± 0.01	0.9	0.8	2.3	96.0	0.0	-0.4
AM6/1-11	Parana do Ramos	Mouth	0.08 ± 0.01	1.3	0.0	1.2	97.5	0.0	-0.7
AM01-21	Madeira	Porto Velho	0.10 ± 0.02	0.1	0.0	0.9	98.9	0.0	-0.8
AM06-35	Madeira	Foz Madeira	0.11 ± 0.02	0.5	0.0	0.9	98.6	0.0	-0.8
AM05-16	Madeira	Foz Madeira	0.08 ± 0.01	0.5	0.0	0.8	98.7	0.0	-0.8
Madeira (Huh et al.)	Madeira	Foz Madeira	0.08 ± 0.01	0.4	0.0	1.1	98.5	0.0	-0.7
Solimoes Basin									
AM08-33	Maranon	Borja	0.12 ± 0.04	0.0	0.0	0.2	85.1	14.6	-0.1
AM08-34	Morona	Mouth	0.17 ± 0.06	0.1	0.0	0.6	79.5	19.9	0.3
AM08-36	Pastaza	Mouth	0.17 ± 0.07	0.1	0.1	0.1	85.1	14.7	-0.1
AM08-38	Huallaga	Mouth	0.05 ± 0.03	0.0	0.6	0.1	97.3	2.0	-0.7
AM08-40	Tigre	Nueva York							
AM08-05	Amazonas	Tamshiyacu	0.16 ± 0.06	0.0	0.2	0.5	98.0	1.3	-0.7
AM08-24	Maranon	San Regis	0.12 ± 0.07	0.0	0.4	0.6	97.1	1.9	-0.6
AM08-13	Ucayali	Jenaro Herrera	0.33 ± 0.11	0.0	0.1	0.5	98.2	1.2	-0.8
AM05-4	Solimoes	Manacapuru	0.14 ± 0.04	0.1	0.1	0.3	92.8	6.7	-0.5
AM06-15	Solimoes	Manacapuru	0.21 ± 0.07	0.1	0.1	0.3	94.9	4.6	-0.6
Solimoes (Huh et al.)	Solimoes	Iquitos	0.13 ± 0.04	0.0	0.1	0.5	95.8	3.6	-0.6
Shield rivers									
AM6/1-20	Tapajós	Mouth	0.20 ± 0.05	1.4	0.0	0.9	30.0	67.7	1.3
Tapajos 19	Tapajós	Mouth	0.22 ± 0.05	1.5	0.0	0.8	30.0	67.7	1.3
AM6/1-13	Trombetas	Mouth	0.33 ± 0.09	2.0	0.0	0.4	30.0	67.6	1.2
Trombetas 15	Trombetas	Mouth	0.42 ± 0.05	2.7	0.0	0.4	30.0	66.9	1.1
Urucara 10	Urucara	Mouth	0.36 ± 0.11	2.0	0.0	0.9	30.0	67.0	1.3
AM6/1-2	Rio Negro	Paricatuba	0.79 ± 0.17	1.1	0.0	0.1	30.0	68.8	1.1
Negro (Huh et al.)	Rio Negro	Paricatuba	0.47 ± 0.03	1.1	0.0	0.2	30.0	68.7	1.1
AM06-20	Rio Negro	Paricatuba	0.65 ± 0.11	1.7	0.0	0.0	30.0	68.4	1.1
AM01-22	Rio Negro	Paricatuba	0.81 ± 0.19	0.9	0.0	0.0	30.0	69.1	1.1
AM01-20	Jaciparana	Mouth	0.17 ± 0.08	0.1	0.0	0.3	30.0	69.0	1.2